The Joint Modes of the Coupled Atmosphere–Ocean System Observed from 1967 to 1986

JIN-SONG XU

Max-Planck-Institut für Meteorologie, Hamburg, Germany

(Manuscript received 6 February 1992, in final form 5 August 1992)

ABSTRACT

Two aspects of the principal oscillation pattern (POP) analysis are used to study the large-scale modes of the coupled atmosphere–ocean system. First, POPs can be considered as the normal modes of the system; one way of studying these normal modes is to estimate them from data. Second, a POP analysis can be viewed as a multivariate spectral analysis and the spectral characteristics of the modes are by-products of the POP analysis. Both aspects are studied using a combined dataset that includes both atmospheric (sea level pressure, 700-mb, and 200-mb zonal winds) and oceanic (sea surface temperature, Pacific sea level, and Pacific subsurface temperature) parameters.

Six joint modes of the coupled atmosphere–ocean system are found in this study. For modes with small eigenvalues, the atmosphere plays an important role. The associated oceanic anomalies appear to be generated by the anomalous atmospheric conditions. For the other modes, which have most of their power on much longer time scales, the ocean is more actively involved. Modes 4 and 5 describe decadal time scale variations. Mode 4 is characterized by changes in SST in all three tropical oceans, and in organized convection over the west Pacific. The results allow us to speculate that these tropical features might excite changes in the extratropical tropospheric and oceanic circulations. Mode 5 shows global-scale SST anomalies and large atmospheric anomalies in the Southern Hemispheric circulation. Mode 6 is the only oscillatory normal mode found in the coupled atmosphere–ocean system; it describes the quasi-cyclic behavior of the El Niño–Southern Oscillation phenomenon.

1. Introduction

The current length of available upper-air atmospheric and subsurface oceanic data records is about 20 to 30 years. These data offer a possibility of constructing a combined dataset for the coupled atmosphere–ocean system. Two kinds of observational studies using (near) global datasets have been performed thus far. The first has been concerned with variability in one or a few of the parameters. The second has concentrated on one particular phenomenon, for example, the El Niño–Southern Oscillation (ENSO). Generally, variability within each dataset is well documented and some phenomena, particular those with shorter time scales, are well described. For variations on decadal time scales, although some aspects are documented, the spatial distributions of such variations are less well known. No studies have systematically considered the joint modes in a *combined* dataset containing both atmospheric and oceanic parameters.

The purpose of this paper is to analyze and to understand the joint modes of the coupled atmosphere–ocean system on time scales of months to years (probably to decades). For this purpose a combined dataset is used that includes ocean temperature, sea level, sea surface temperature (SST), sea level pressure (SLP), and low- and high-level zonal winds. To identify signals within the atmosphere–ocean system, a principal oscillation pattern (POP) analysis is used. The technique was introduced by Hasselmann (1988) and Storch et al. (1988). Its success in capturing the spatial and temporal characteristics of one or more signals in a dataset was shown by, among others, Xu and Storch (1990) and Xu (1992). In this paper, the POP analysis is described only briefly. In section 2, two aspects of the POP analysis are emphasized that are crucial for this paper, but were not explicitly used in the earlier studies. Some ideas which can be used to specify the physical processes involved in each signal are described in section 3. Data and data processing are described in section 4. The joint modes that are found are presented and discussed in section 5. Conclusions are given in section 6.

2. Identifying the signals: The POP analysis

a. POPS as estimated normal modes

The following notation is used: vectors are given in bold and matrices in san serif. The symbol T denotes transpose; * represents the complex conjugate.

The POP formalism assumes that an m-dimensional state vector $\mathbf{x}(t)$ is modeled by a linear equation,

$$\mathbf{x}(t+1) = \mathsf{B}\mathbf{x}(t) + \mathbf{n}(t), \qquad (1)$$

Corresponding author address: Jin-Song Xu, Max-Planck-Institut für Meteorologie, Bundesstrasse 55, Hamburg 13, FRG, D-2000.

where **B** is the system matrix and $\mathbf{n}(t)$ represents the noise time series. The eigenvectors of **B** are POPs. According to this definition, POPs are formally the normal modes of system (1).

Generally **B** is not symmetric so that the eigenvectors **P** and their eigenvalues λ are either real or appear in conjugate pairs. The state of $\mathbf{x}(t)$ may be described by the m POPs $\mathbf{P}_j$:

$$\mathbf{x}(t) = \sum_{j}^{m} z_j(t)\mathbf{P}_j, \tag{2}$$

where $z_j(t)$ is the coefficient time series of the corresponding pattern $\mathbf{P}_j$.

Because the eigenvector of a matrix is only defined to an arbitrary factor $ce^{i\theta}$ (for real eigenvector $\theta = 0$), we need to choose some standard normalization for the POPs. In this study, c is chosen so that the length of (real or imaginary part of) the eigenvector is equal to m. The strength of mode $\mathbf{P}_j$ is then given by the amplitude of $z_j(t)$. For a complex POP, θ must also be specified (see section 5).

According to (2), a signal in the form of $z_j(t)\mathbf{P}_j$ has the same unit as in $\mathbf{x}(t)$, that is, if $\mathbf{x}(t)$ represents temperature anomalies in °C, $z_j(t)\mathbf{P}_j$ gives temperature anomalies in °C for the considered jth signal. This notion is frequently used in section 5.

Because of the linear assumption made in (1), the evolution of coefficients is given by

$$z_j(t+1) = \lambda_j z_j(t) + n_j(t), \tag{3}$$

where $n_j(t)$ is related to $\mathbf{n}(t)$.

b. *POP analysis as multivariate spectral analysis*

Equation (3) can also be restated in the frequency domain. After some manipulations, the autospectrum $\Gamma_{z_j}(\omega)$ of the POP coefficient time series $z_j(t)$ can be written

$$\Gamma_{z_j}(\omega) = \frac{\Gamma_{n_j}(\omega)}{(e^{i\omega} - \lambda_j)(e^{i\omega} - \lambda_j)^*}, \tag{4a}$$

where $\Gamma_{n_j}(\omega)$ is the autospectrum of the noise, $n_j(t)$. The autospectrum $\Gamma_{z_j}(\omega)$ is a function of the noise autospectrum $\Gamma_{n_j}(\omega)$ and the eigenvalue λ_j. If the POPs in Eq. (2) capture all signals in the data $\mathbf{x}(t)$, $\Gamma_{n_j}(\omega)$ should be white or at least smooth. In this study, the noise time series are also calculated (not shown) and are white. Equation (4a) then presents different types of spectra depending on the magnitude of λ and whether λ is complex or real. In the following $|\lambda| < 1$ is considered, which is usually true for stationary time series.

1) PEAK SPECTRUM (λ IS COMPLEX AND $|\lambda| \to 1$)

This type of spectrum is obtained when an eigenvalue is complex, that is, $\lambda_j = |\lambda_j| e^{i\phi_j}$. For $|\lambda_j| = 1$, a resonance peak occurs for $\omega = \phi_j$. For $|\lambda_j| < 1$, spectrum (4a) exhibits a maximum centered at frequency ϕ_j with width determined by $|\lambda_j|$. The smaller $|\lambda_j|$ is, the broader the maximum is. Therefore, the eigenvalue determines not only the oscillation frequency but also the width of the spectral peak.

For a complex POP $\mathbf{P} = \mathbf{P}_j^{re} + i\mathbf{P}_j^{im}$; if $|\lambda_j|$ is near 1, the signal identified by the POP describes the oscillatory tendency[1]:

$$\begin{array}{ccc} & \mathbf{P}_j^{im} & \\ \nearrow & & \searrow \\ -\mathbf{P}^{re} & & \mathbf{P}_j^{re}, \\ \nwarrow & & \swarrow \\ & -\mathbf{P}_j^{im} & \end{array} \tag{5}$$

with oscillation period $T_j = 2\pi/\phi_j$ and e-folding time $-(\ln |\lambda_j|)^{-1}$.

2) RED NOISE SPECTRUM ($\lambda \to 1$) AND WHITE NOISE SPECTRUM ($\lambda \to 0$)

In the case of a real eigenvalue, equation (4a) can be rewritten:

$$\Gamma_{z_j}(\omega) = \frac{\Gamma_{n_j}(\omega)}{(1 - 2\lambda_j \cos\omega + \lambda_j^2)}, \tag{4b}$$

which describes a red noise spectrum when $\lambda_j \to 1$, and a white noise spectrum when $\lambda_j \to 0$.

Equations (4a) and (4b) show that the POP analysis can be considered as a "multivariate spectral analysis," which isolates multivariate signals, that is, patterns across the whole available frequency interval [in this study from $(2\ \text{month})^{-1}$ to $(20\ \text{yr})^{-1}$]. In optimal cases, the extensive second moment information in the high-dimensional $\mathbf{x}(t)$ can be compressed into a manageable set of numbers (λ_j) and patterns (POPs).

The POP analysis is not only useful for estimating normal modes of data, but also provides a simple diagnostic tool for expressing the spatial and spectral characteristics of these modes.

3. Specifying physical processes

Although the POP analysis provides an easy answer to the question of what the normal modes of a system look like, the results of a POP analysis do not suggest what physical mechanism is involved in each mode.

The basic idea for specifying physical processes is to specify relationships between well-known processes and

[1] Equation (3) describes an anticlockwise rotation in the 2D complex plane. However, for a complex POP, the signal is represented by $z\mathbf{P} + z^*\mathbf{P}^* = 2z^{re}\mathbf{P}^{re} - 2z^{im}\mathbf{P}^{im}$, where $\mathbf{P}^{re}$ and z^{re} ($\mathbf{P}^{im}$ and z^{im}) are the real (imaginary) parts of the complex POP and POP coefficient. In practice, $2z^{re}$ and $-2z^{im}$ are used to describe the time evolution of signals **P** and $\mathbf{P}^*$ ($2z^{re}$ and $-2z^{im}$ are noted hereafter as the real and imaginary parts of the POP coefficient). Therefore, clockwise rotation as given in (5) is observed.

their corresponding anomaly distributions. Joint modes of the coupled atmosphere–ocean system are considered in this study and the concentration is mainly on the air–sea processes. In the following discussion, SST is considered as one possible forcing for the atmosphere, while sea level and subsurface temperature are treated as indicators of oceanic response to atmospheric forcing. The low- and high-level atmospheric parameters are used to describe the vertical structure of the atmospheric response to oceanic forcings.

a. Extratropical SST and the overlying atmosphere

In the extratropics, two kinds of SST patterns associated with two different air–sea processes have been observed and investigated by numerical studies.

First, if the atmosphere forces the ocean, it would be expected that in the presence of an anomalous anticyclone over the North Atlantic or North Pacific the SST pattern would show anomalous warming at the anticyclone's western and southern flank and cooling at its eastern and northern flank (see also Fig. 1b) in Zorita et al. 1992). It is generally understood that the SST anomalies are produced by the warm marine and cold continental air advection brought about by the anomalous atmospheric circulation. This process was first proposed by Bjerknes (1962) and is supported by a GCM study for the North Pacific (Luksch and Storch 1992). Because the warm marine and cold continental air advection is strongest during wintertime, the above-mentioned air–sea process is strongest during wintertime.

In the second case, if the ocean forces the atmosphere, it would be expected that downstream of the positive SST anomalies the low-level atmosphere would become warmer and wetter, and negative SLP anomalies would be observed east of the SST anomalies (see also Fig. 1a in Zorita et al. 1992). This process, in which anomalous heating is balanced by horizontal advection of temperature, was proposed by Egger (1977) and Webster (1981).

Other processes may of course be responsible for extratropical SST anomalies, but only the above-mentioned two processes are considered here.

b. Tropical SST and the overlying atmosphere

In the tropics, anomalous heating is generally associated with an air–sea interaction process with positive feedback. The atmospheric response to local heating involves large-scale convection over the forcing area as already indicated by a simple model (Gill 1980). The atmospheric anomalies in turn favor the SST anomalies, so that more SST anomalies can be produced. In this pattern of tropical air–sea interaction processes, only local heating anomalies are considered. It is not clear, for instance, how the atmosphere would react if the whole tropics were warmer.

c. Sea level and the overlying atmosphere

If slow processes (changes in the shape of the ocean, or land uplift or sinking) are neglected, sea level variation μ' can be written as the sum of three processes (Gill and Niiler 1973):

$$\mu' = \mu'_a + \mu'_s + \mu'_m. \tag{6}$$

The first term on the right-hand side, μ'_a, is a direct local sea level response to the atmospheric pressure anomalies known as the inverse barometric effect. An increase of atmospheric pressure of 1 mb produces a 1-cm depression of the sea level.

The second term, μ'_s, describes sea level changes caused by changes in the density of the column which imply an expansion or contraction of the column. Because of the strong relation between μ'_s and heat and freshwater fluxes, which are not available for this study, the second term in Eq. (6) is not considered.

The μ'_m term describes the sea level changes associated with motions in the upper layers of the ocean, which, except on the equator, are related to current anomalies in the upper layers of the ocean via the geostrophic relation. In this study, only wind-driven motions are considered. Away from coast, upper-layer motions are largely induced by wind forcing via the Sverdrup relation. We assume that changes in the western boundary current can be implicitly derived from interior flow changes, that is, an anomalous southward (northward) interior flow is associated with an anomalous northward (southward) return flow on the western boundary. On the equator, other effects such as Ekman flux (pumping) or equatorial waves become dominant for sea level changes.

The barometric μ'_a is mainly forced *locally* by the atmospheric pressure. On the other hand, the response of sea level to motions is *not local* and, in the presence of large-scale wind stress curl anomalies, it can be even basinwide.

d. Oceanic response in the upper 200 meters

Different vertical structures of oceanic anomalies can be produced by changes in the structure of the mixed layer and the thermocline, and by reaction of the ocean in terms of barotropic and baroclinic modes. Although subsurface temperatures are used in this study, they are not sufficient for determining these physical processes. Therefore, no further attempt is made to clarify causes of vertical structure of oceanic anomalies.

The summarized air–sea processes and their anomaly distributions are used in section 5 as a guide for understanding the joint modes of the atmosphere–ocean system.

4. Data

The data used in this paper are monthly anomalies of:

(i) Sea surface temperature (SST) on a 4° lat by 10° long grid from the Comprehensive Ocean–Atmospheric Data Set (COADS) (Woodruff et al. 1987) prepared by P. Wright (Wright et al. 1988).

(ii) Pacific Ocean temperature at 10-, 50-, 125-, and 200-m depth on a 5° lat by 10° long grid as archived at Far Seas Fisheries Research Laboratory, Japan, and at the Scripps Institution of Oceanography, La Jolla, California. The data are derived from 1° × 1° XBT measurements taken at 12 levels and between the surface and about 250 meters. The original bimonthly data are interpreted into monthly data via a simple time-average procedure. In this paper, (i) and (ii) provide the dataset for ocean temperature.

(iii) Sea level station data in the Pacific collected by Wyrtki et al. (1988).

(iv) A combined dataset of SLP including the Northern Hemisphere SLP (20°N–50°N) stored at the National Center for Atmospheric Research, Boulder, Colorado; Southern Hemisphere SLP (10°S–40°S) generated at the Bureau of Meteorology Research Center, Melbourne, Australia; and the tropical (20°N–20°S) COADS SLP (Wright et al. 1988).

(v) Zonal winds at 200 and 700 mb from the National Meteorological Center analysis, Washington, D.C., which are longitudinally smoothed resulting in a 10° zonal resolution. The north–south resolution is unchanged with a meridional resolution of about 3.5° at 40°, and 5° in the equatorial region.

The dimension of each dataset considered in this paper is of the order of 10^2 to 10^3. The order of the system matrix $\mathbf{B}$ in Eq. (1) for the combined dataset would then be 10^3. To simplify the interpretation of 10^3 POPs and to concentrate on the large-scale variations, each dataset is compressed into a smaller space spanned by the first few empirical orthogonal functions (EOFs). No effort is made to check the significance of the EOFs. Because the error in estimating the higher-order EOFs is much larger than that of the lower-order EOFs, only EOFs that explain more than 1% of the total variance are used in this study. The dimension of the combined system $\mathbf{x}(t)$ is then 95. The data information and results of the data compression are shown in Table 1.

The 95D combined system is further compressed into the space spanned by the first nine EOFs of this system. These EOFs, whose principal components are the input vector time series $\mathbf{x}(t)$ for the POP analysis, explain 56% of the variance of the combined dataset and about 45% of the original dataset. The results obtained within the 9D space are then translated back into the physical space. The EOF compression from a dimension of 4127 for the original datasets, to 95 for the combined dataset, and to 9 for a subspace of the combined dataset can be interpreted as a two-step spatial filter: in the first step from a dimension of 4127 to 95, small-scale variations within *each* dataset are compressed, and in the second step from a dimension of 95 to 9, small-scale variations within the *combined* dataset are compressed. Therefore, the POPs identified from spatially filtered data are *large-scale* joint modes of the coupled air–sea system.

TABLE 1. Information on dimensions of the datasets, numbers of EOFs used for the combined dataset, and variance explained by these EOFs for each dataset.

Datasets used	Dimensions of the original datasets	No. of EOF used for the combined dataset	Variance explained by these EOFs
i and ii	1061	25	71%
iii	79	21	92%
iv	1331	23	81%
v	1656	26	76%
sum	4127	95	80% (averaged)

In this paper the variances of the oceanic and atmospheric data are adjusted so that they are equal. This crude treatment is necessary because of the inhomogeneity of the data. As shown in Table 1, the dimension of the atmospheric data (2987) is much larger than that of the oceanic data (1140). Without any weighting procedure, the ratio of the low-frequency signals in which we are interested to the high-frequency atmospheric noise would be much higher. We suggest that the use of the weighting procedure increases the power of the analysis technique in isolating the low-frequency modes.

Because datasets (i) and (v) begin in 1967 and 1968, and (iii) in 1975, and most of the datasets end in 1986, the time period of the combined dataset is chosen to be 1967 to 1986. In order to study the variability of the combined dataset across the whole available frequency interval, *no time filtering* is done.

Rather than filling missing data by interpolation, the missing data are ignored in the EOF and POP calculation. Thus, each matrix element is estimated individually. The principal components $\alpha_i(t)$ for EOF $\mathbf{e}_i$ are estimated according to a least-squares fit by

$$\alpha_i(t) = \frac{\mathbf{e}_i^{\mathrm{T}} \cdot \mathbf{x}(t)}{\mathbf{e}_i^{\mathrm{T}} \cdot \mathbf{e}_i}. \tag{7}$$

5. Results

In the 9D subspace, two complex POPs together with their complex conjugates and five real POPs are found. One of the complex POPs has eigenvalue $\lambda = 0.5\, e^{i2\pi(103)^{-1}}$, but the coefficient time series has most of its power at a frequency much higher than (103 months)$^{-1}$. Thus, Eq. (5) is not a valid interpretation, and this mode is not considered in the following discussion. The eigenvalues of the other six POPs are listed in Table 2.

To test the stability of the results, the POP analysis is also performed using different numbers of EOFs. It

TABLE 2. Eigenvalue of each POP and standard deviation δ of each POP coefficient time series. For the complex mode 6, standard deviations of the real and imaginary part of the coefficient are shown. The standard deviations δ are used in section 5 to estimate the averaged strength of each mode.

	λ_j	Standard deviation δ_j
Mode 1	0.15	0.05
Mode 2	0.40	0.09
Mode 3	0.66	0.05
Mode 4	0.86	0.07
Mode 5	0.92	0.06
Mode 6	$0.93e^{i2\pi(51)^{-1}}$	$0.11\ (0.10)^{-1}$

turns out that in all these cases only six POPs are interpretable. In the following the six signals $\mathbf{P}_j$ (j = 1, · · · 6) identified by the five real POP and one complex POP listed in Table 2 are considered.

The eigenvalues indicate two white spectra with $|\lambda_{1,2}|$ = 0.15, 0.4, and one spectrum with λ_3 = 0.66; two red spectra with $|\lambda_{4,5}|$ = 0.86, 0.92, and one with a spectral peak around 51 months and an e-folding time of about 12 months. Figures 1 and 2 show the POP coefficient time series and the spectra derived from the time series. As expected, both Figs. 1 and 2 confirm the spectral characteristics suggested by the eigenvalues. The oscillation period for the complex POP is about 40 months in Fig. 2f and is, therefore, overestimated by the complex eigenvalue.

Because the POPs have equal magnitudes (section 2), the strength of each signal $z_j(t)\mathbf{P}_j$ is indicated by the amplitude of the corresponding POP coefficient time series (Fig. 1). The standard deviation of these time series (Table 2) suggests that in the combined dataset mode 6 is the strongest signal, followed by modes 2 and 4, and modes 1, 3, and 5 are the weakest signals.

In the following, two diagrams are usually shown for each POP, one for the atmospheric part of a POP (SLP, 700-mb, and 200-mb zonal wind), and the second for the oceanic part of a POP (SST, Pacific subsurface temperature, and sea level). For some of the signals, one or two parameters are not shown. In this case the variability in the missing variable is negligible or provides the same information as other parameters, and is therefore not presented.

a. Joint modes: Mode 1, mode 2, and mode 3

As will be shown shortly, the three modes with smaller eigenvalues (Table 2 and Fig. 2a–c) have many features in common. For this reason they are considered together in this section.

1) CENTERS OF ACTION

The centers of action of each mode can be identified by the regions of large explained variances, which are about 20% for the atmospheric parameters and about 5%–10% for the oceanic parameters (shaded in Fig. 3, Fig. 4, and Fig. 5). All three modes are confined to the Northern Hemisphere: Mode 1 in the North Atlantic (Fig. 3), mode 2 in the North Pacific (Fig. 4), and mode 3 in the region from the central North Pacific to the North Atlantic (Fig. 5).

Although the wind field and the SLP field extend only to about 50°N, Figs. 3, 4, and 5, respectively, bear strong resemblance to the "Pacific/North American"

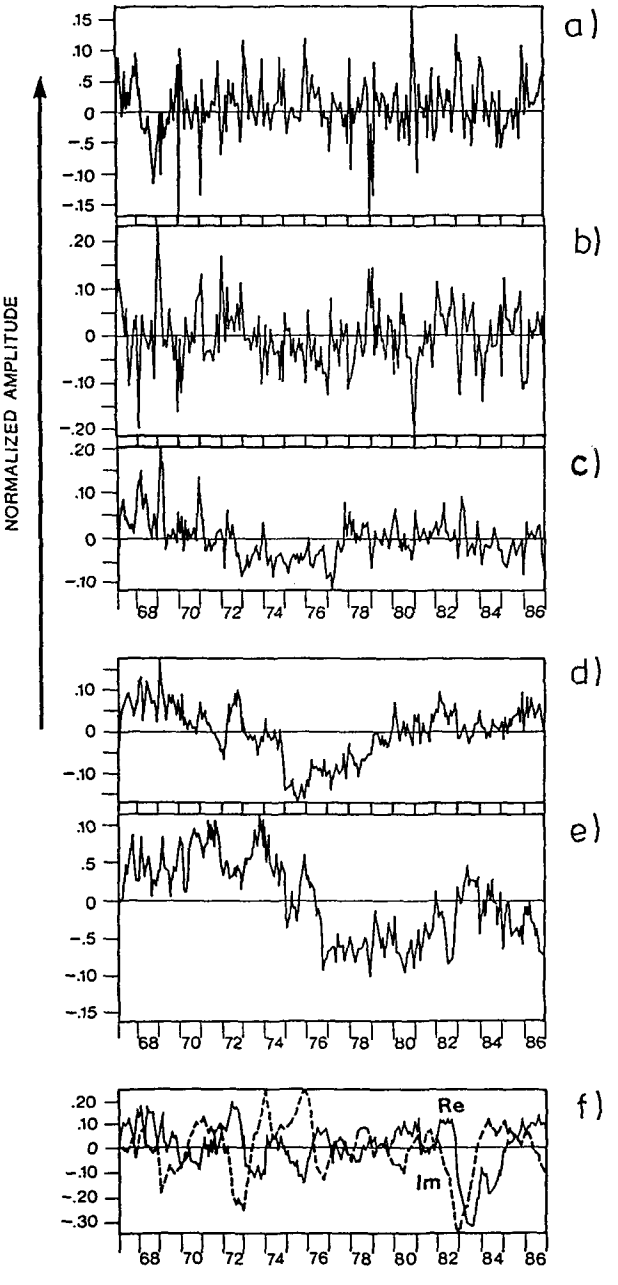

FIG. 1. POP coefficient time series of mode 1 to mode 6 as listed in Table 2. Because the POPs are normalized in such way that their magnitudes are equal, the amplitude of the POP coefficient time series indicates the strength of each corresponding mode.

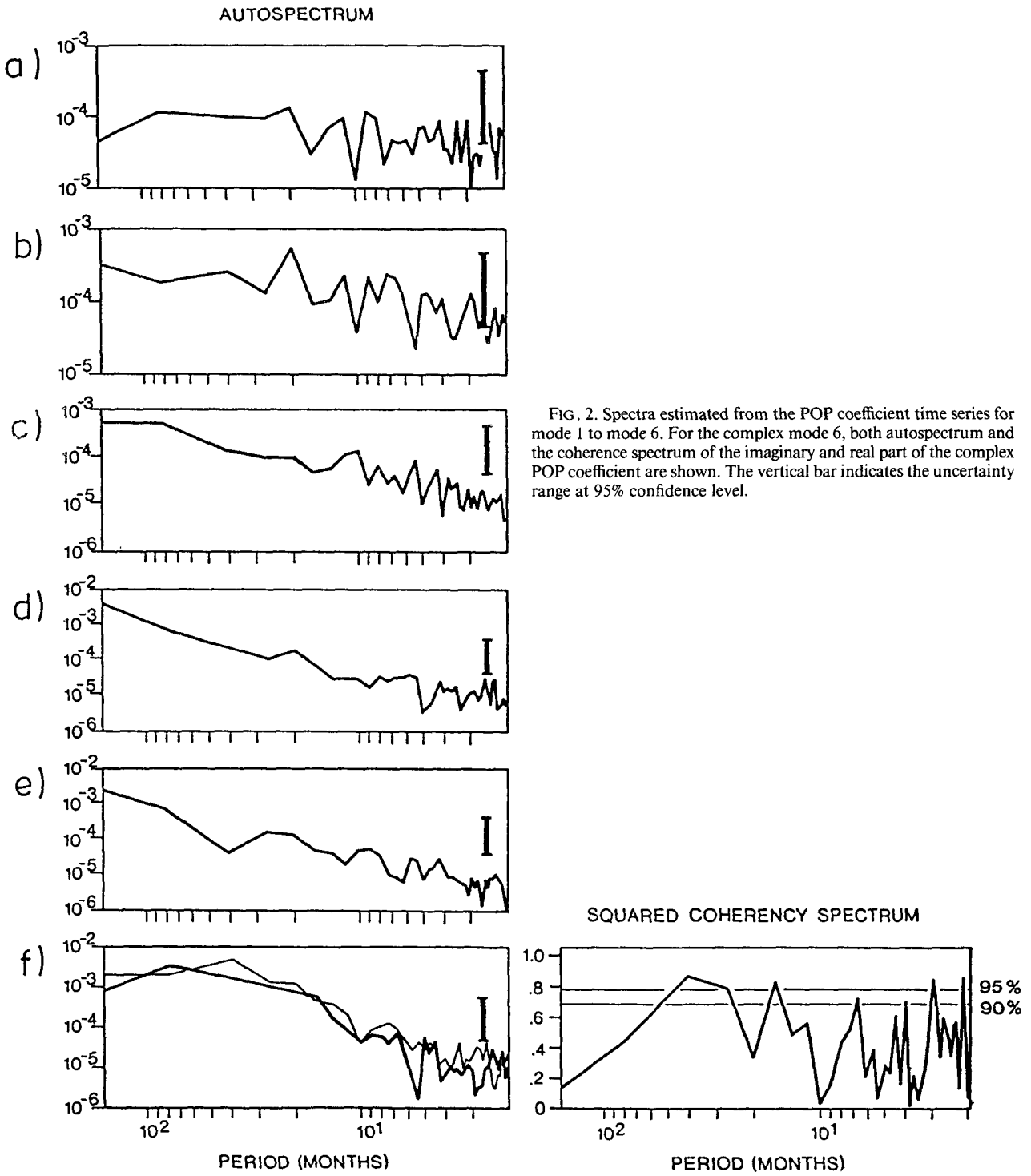

FIG. 2. Spectra estimated from the POP coefficient time series for mode 1 to mode 6. For the complex mode 6, both autospectrum and the coherence spectrum of the imaginary and real part of the complex POP coefficient are shown. The vertical bar indicates the uncertainty range at 95% confidence level.

(PNA), "east Atlantic" (EA), and "west Atlantic" (WA) teleconnection patterns noted by Wallace and Gutzler (1981). Similar to EA and WA, modes 1 and 3 describe north–south seesaws over the North Atlantic with the seesaw center in mode 1 being shifted southeastward relative to that in mode 3.

For each mode, the POP patterns for 700- and 200-mb zonal wind are nearly identical (not shown), indicating that these modes are barotropic.

2) SEASONAL DEPENDENCE

All three of these modes show strong seasonal dependence. Figure 6 gives a frequency distribution of

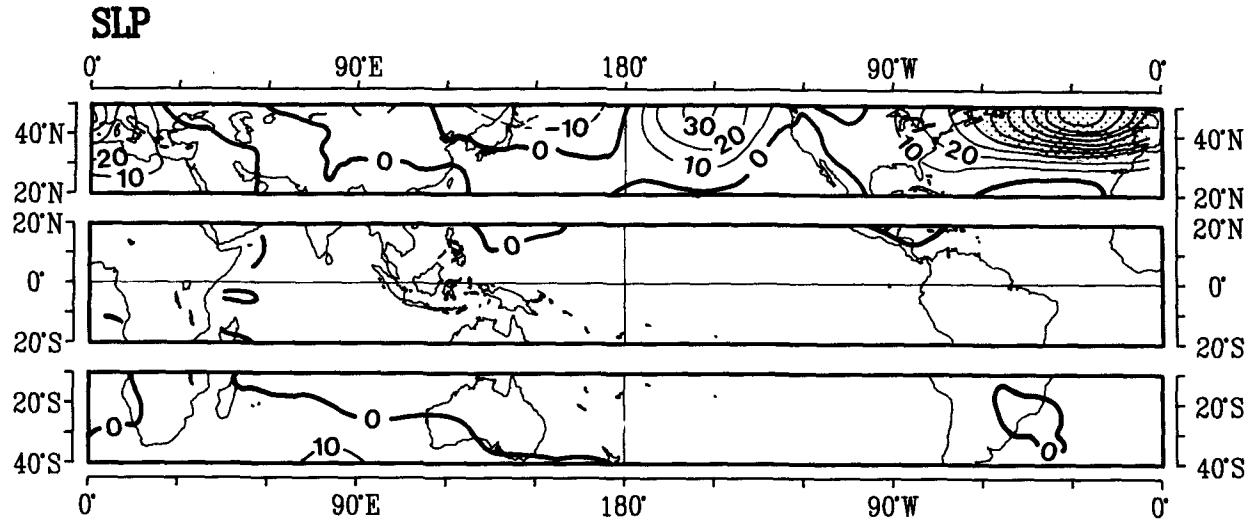

FIG. 3. POP pattern of mode 1 for the sea level pressure (mb). Shaded area indicates explained variance larger than 20%.

the three POP coefficients larger than one standard deviation in each calendar month and shows that strong positive and negative amplitudes of these modes occur mostly during Northern Hemisphere winter.

3) THE ROLE OF ANOMALOUS WARM AND COLD AIR ADVECTION

For mode 2 with a positive coefficient, positive SLP anomalies (Fig. 4) and anomalous anticyclonic flow are found in the North Pacific area. The SST anomalies shown in Fig. 7 are positive over the North Pacific near 40°N, that is, at the western and southern flanks of the anticyclone which is indicated by the arrow, and negative in the east North Pacific and along the North American coast, that is, at the anticyclone's eastern and northern flank. Considering the seasonal dependence of this mode, the spatial distributions of SST anomalies fit the process associated with warm and cold air advection, rather than the process proposed by Egger and Webster.

For modes 1 and 3, the role of anomalous warm and cold air advection, as indicated by the arrows in Figs. 8 and 9, can also be identified. The results suggest that the anomalous heat fluxes associated with the anomalous warm and cold air advection are responsible for the large-scale SST changes for all three modes.

4) INVERSE BAROMETRIC EFFECT

In mode 2, large sea level anomalies (Fig. 7) are found directly below the anomalous anticyclone in Fig. 4. The maximal pressure anomaly given by $z_2\mathbf{P}_2$ is about 9 mb (with z_2 = one standard deviation δ_2

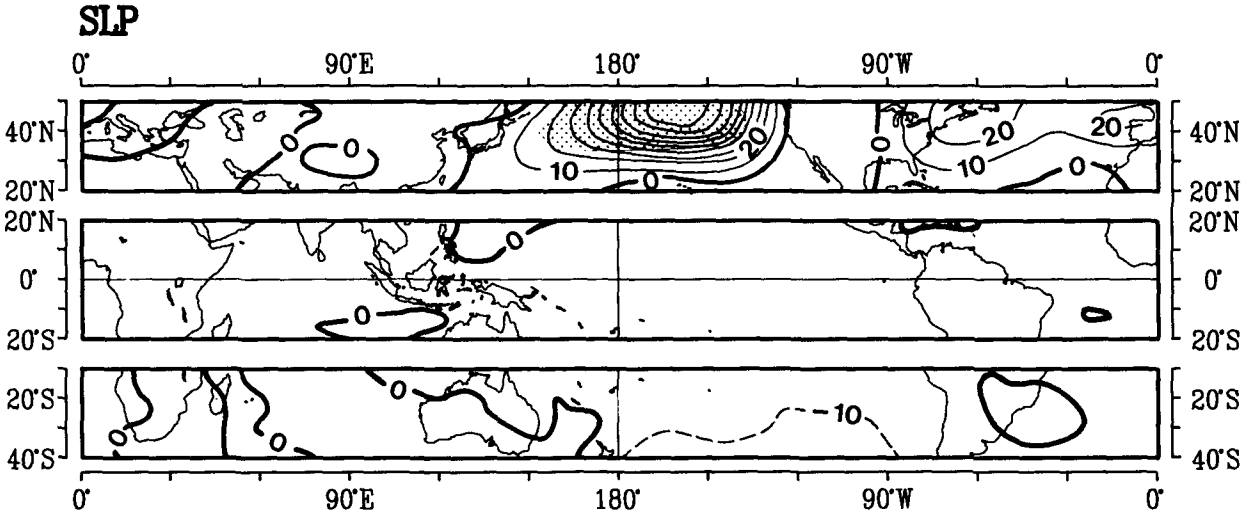

FIG. 4. POP pattern of mode 2 for the sea level pressure (in mb). Shaded area indicates explained variance larger than 20%.

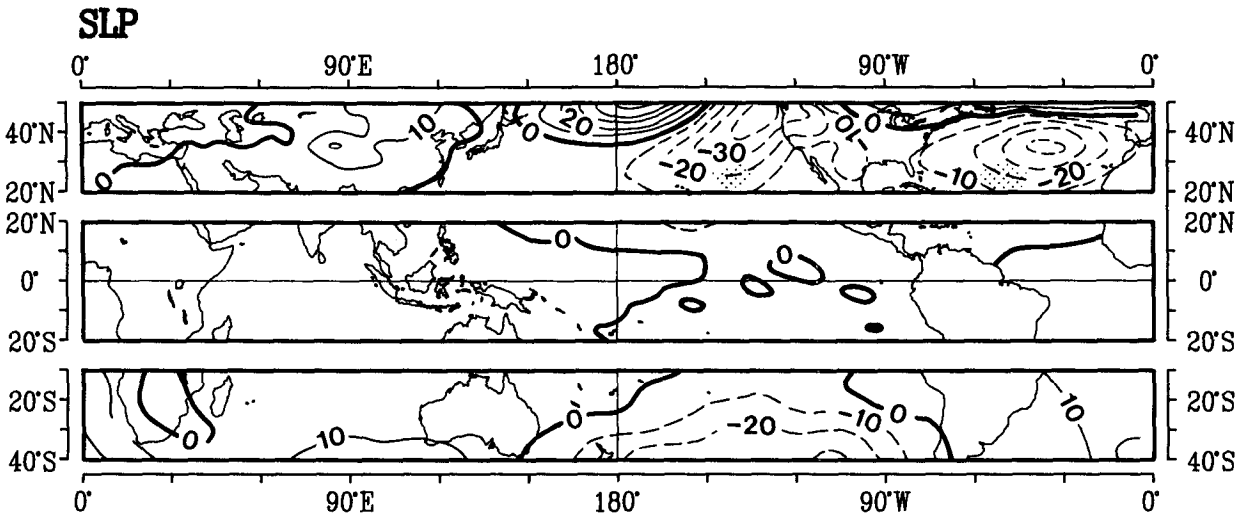

FIG. 5. POP pattern of mode 3 for the sea level pressure (mb). Shaded areas indicate explained variance larger than 20%.

= 0.09, and P_2 = 100 mb), which is roughly balanced by the largest sea level anomaly of about −11 cm (with $z_2 = \delta_2 = 0.09$, $P_2 = -1219$ mm). The inverse barometric effect seems to be the dominant effect for sea level anomalies shown in Fig. 7. For modes 1 and 3, no sea level data are available over the Atlantic.

5) ORIGIN OF THE SIGNALS

In a theoretical normal-mode study, Simmons et al. (1983) suggested that the origin of the teleconnection patterns lies in the atmosphere. Consistent with their suggestion, our study shows further how the atmospheric and oceanic anomalies of these modes are related to each other. According to such relationship, we speculate that the internal dynamics of the atmosphere generates such patterns, and the ocean acts only passively.

Because the teleconnection patterns vary on month-to-month time scales (Simmons et al. 1983) and the oceanic reaction time to the atmospheric pressure anomalies and the anomalous warm and cold advection is short (a period of months), we suggest that for mode 3, which is supercomposed to a long-term vari-

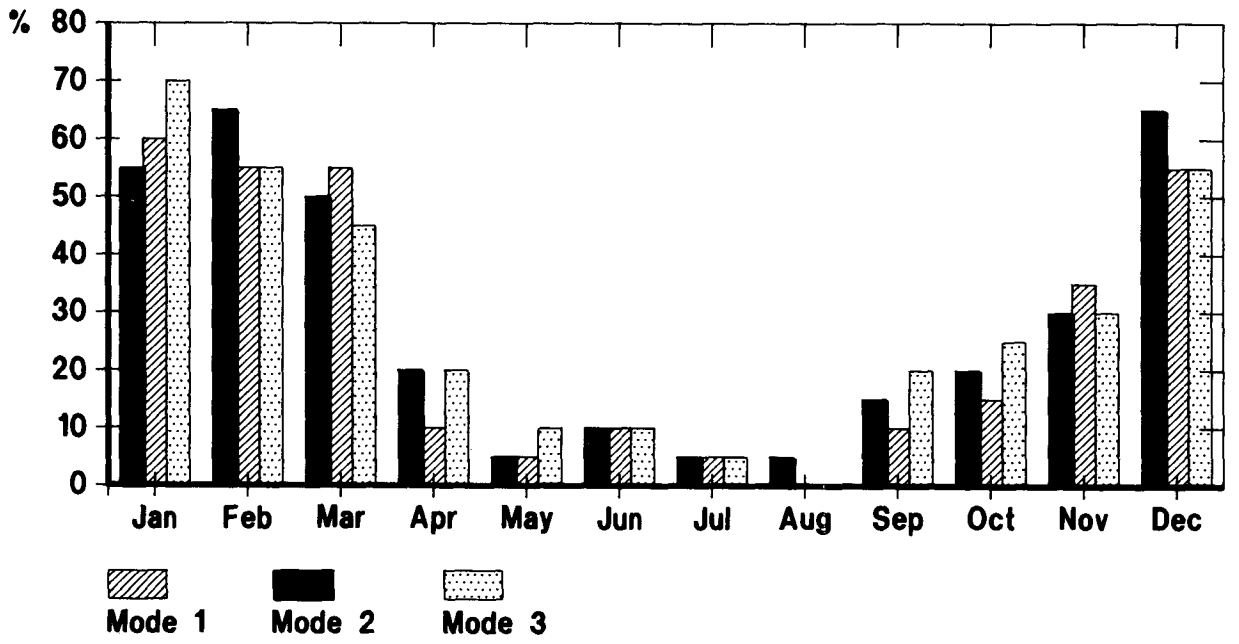

FIG. 6. Frequency distribution of POP coefficients larger than one standard deviation for each calendar month.

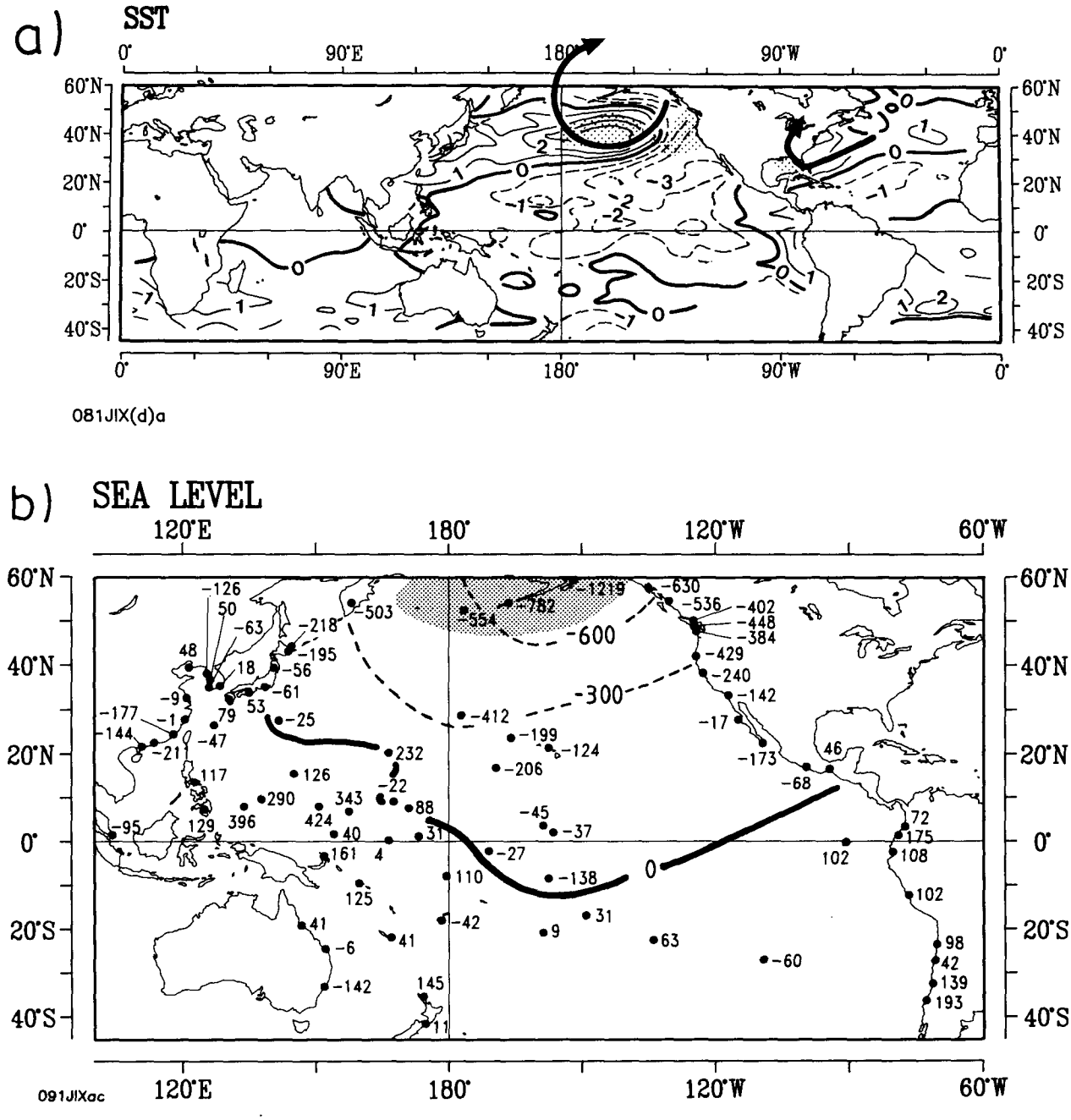

FIG. 7. POP pattern of mode 2 for (a) sea surface temperature (°C), and (b) sea level (mm). Shaded areas indicate explained variance larger than 5% for SST and 10% for sea level.

ation [slight decrease of the amplitude of $z_3(t)$ from the late sixties to about 1976/77 in Fig. 1], some other processes must generate the low-frequency part of the mode.

b. The joint mode on decadal time scales: Mode 4

1) TROPICAL FEATURES

The most striking features of this mode are the large positive SST anomalies in all tropical oceans (Fig. 10a) with maximum SST values in the western Pacific on the equator and in the subtropical Pacific and weak anomalies along the equator in the eastern Pacific. The coefficient time series of this mode (Fig. 2d) indicates variation on a decadal time scale. The increase of the amplitude of the POP coefficient time series since 1975 together with the positive sign of SST anomalies describes a pronounced increase of SST in the global tropical ocean up to several tenth °C.

In the atmosphere, in view of the evidence that SSTs

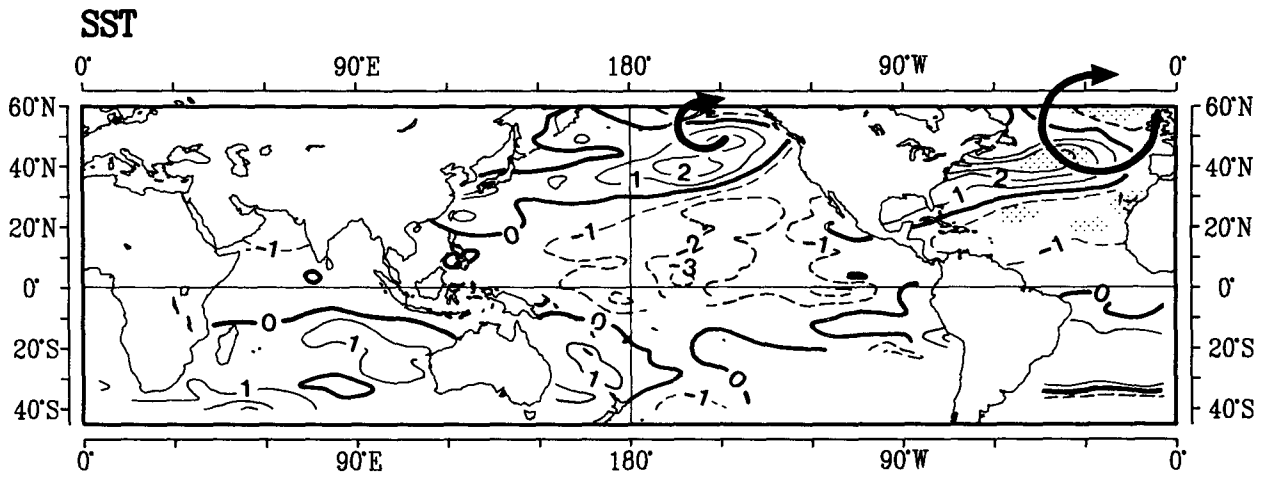

FIG. 8. POP pattern of mode 1 for sea surface temperature (°C). Shaded areas indicate explained variance larger than 3%.

in excess of approximately 28°C are required to support organized convection and the fact that the SST anomalies of this mode have rather small amplitude, the convection induced by this mode is expected to be found only over the Indonesian region and the east Pacific where, in the climatological mean, SSTs of about 28°–29°C exist. Indeed, the most pronounced atmospheric feature in the tropics (Fig. 11) is the anomalous convergent (divergent) flow over the Indonesian region and the west Pacific at 700 mb (200 mb) as indicated by the westerly (easterly) anomalies over the Indian Ocean and the easterly (westerly) anomalies over the Pacific in Fig. 11. These patterns lead to the suggestion that the tropical atmosphere does respond to small-amplitude variations of the tropical SST forcing (up to a few tenths of a degree Celcius) and displays organized convection centered over the Indonesian region and the west Pacific. Figure 2d further indicates that this convective motion has increased since the mid-1970s.

For the upper layer of the tropical Pacific, Fig. 10b shows out-of-phase anomalies with positive values in the first 50 meters and negative values in the layers below in the west Pacific. This vertical structure is different from that observed during ENSO (Fig. 17b).

2) EXTRATROPICAL FEATURES

The largest extratropical atmospheric anomalies are the anomalous westerlies over the central North Pacific and anomalous easterlies over the northern North Pacific at both 700 mb and 200 mb (Fig. 11). Note that the explained variance for the North Pacific zonal wind is not located in the regions of anomaly maximum.

Large SST anomalies with large negative values zonally oriented along 40°N and large sea level anom-

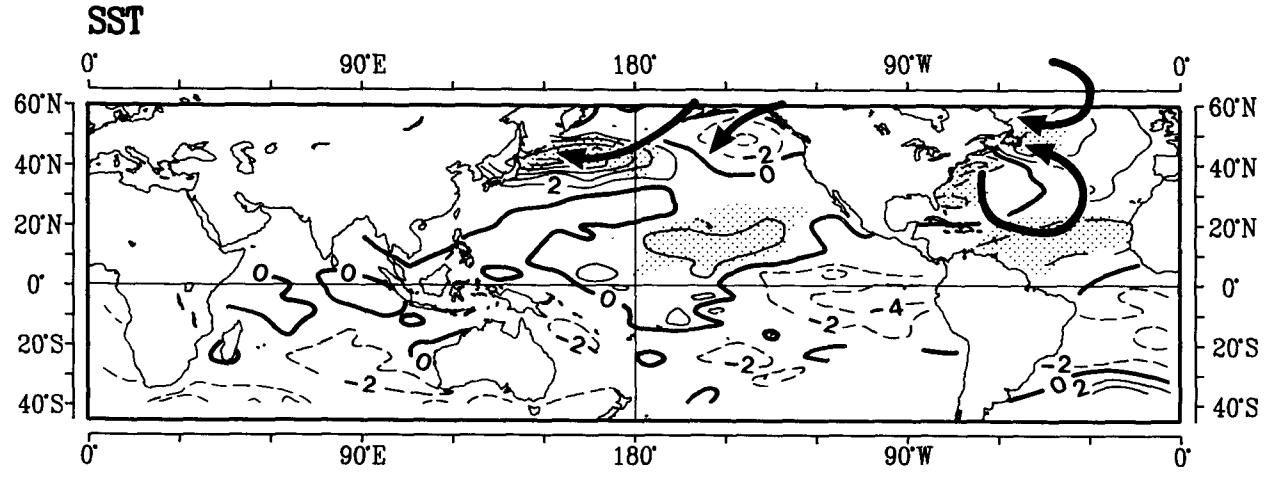

FIG. 9. POP pattern of mode 3 for sea surface temperature (°C). Shaded areas indicate explained variance larger than 5%.

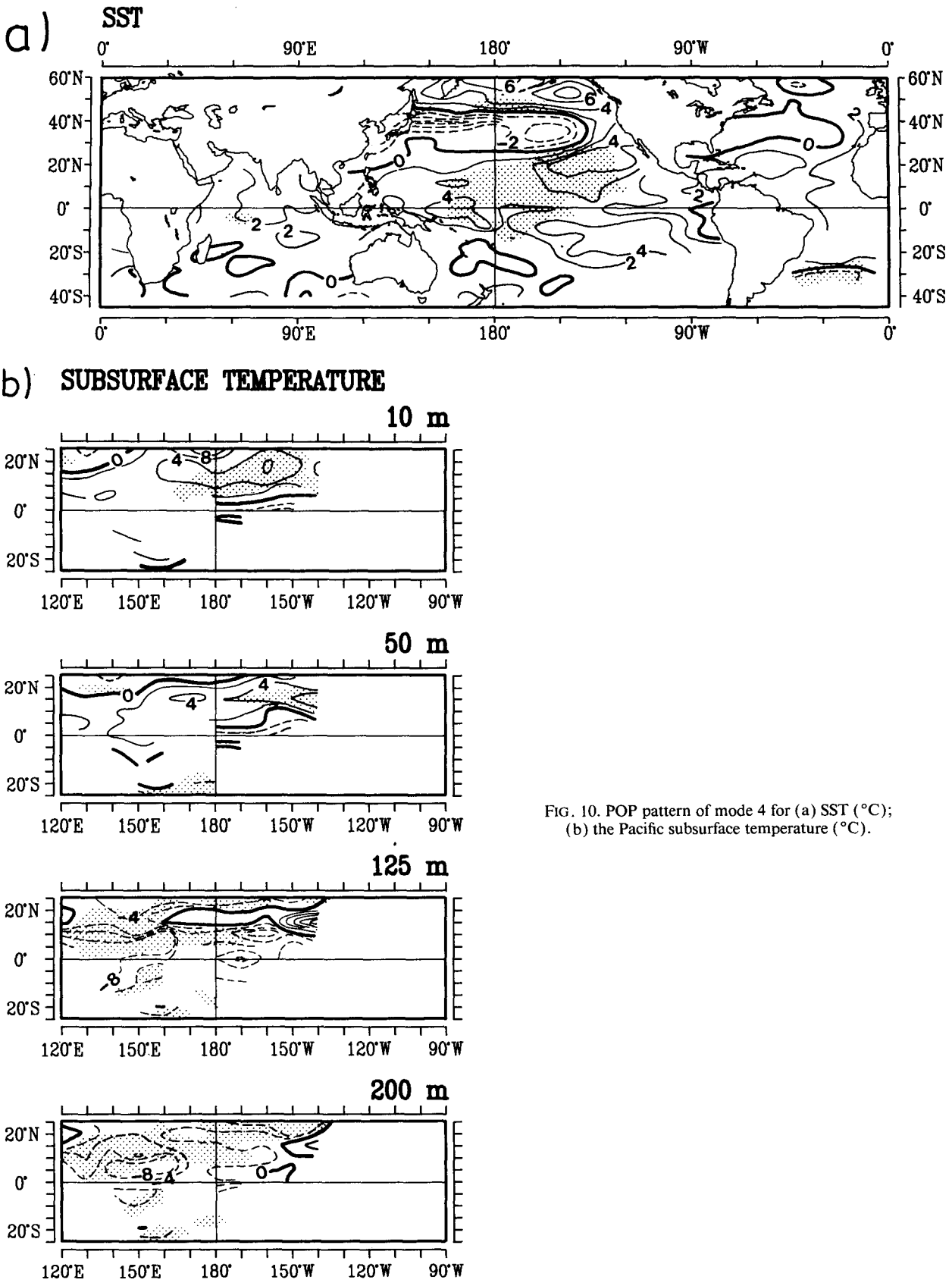

FIG. 10. POP pattern of mode 4 for (a) SST (°C); (b) the Pacific subsurface temperature (°C).

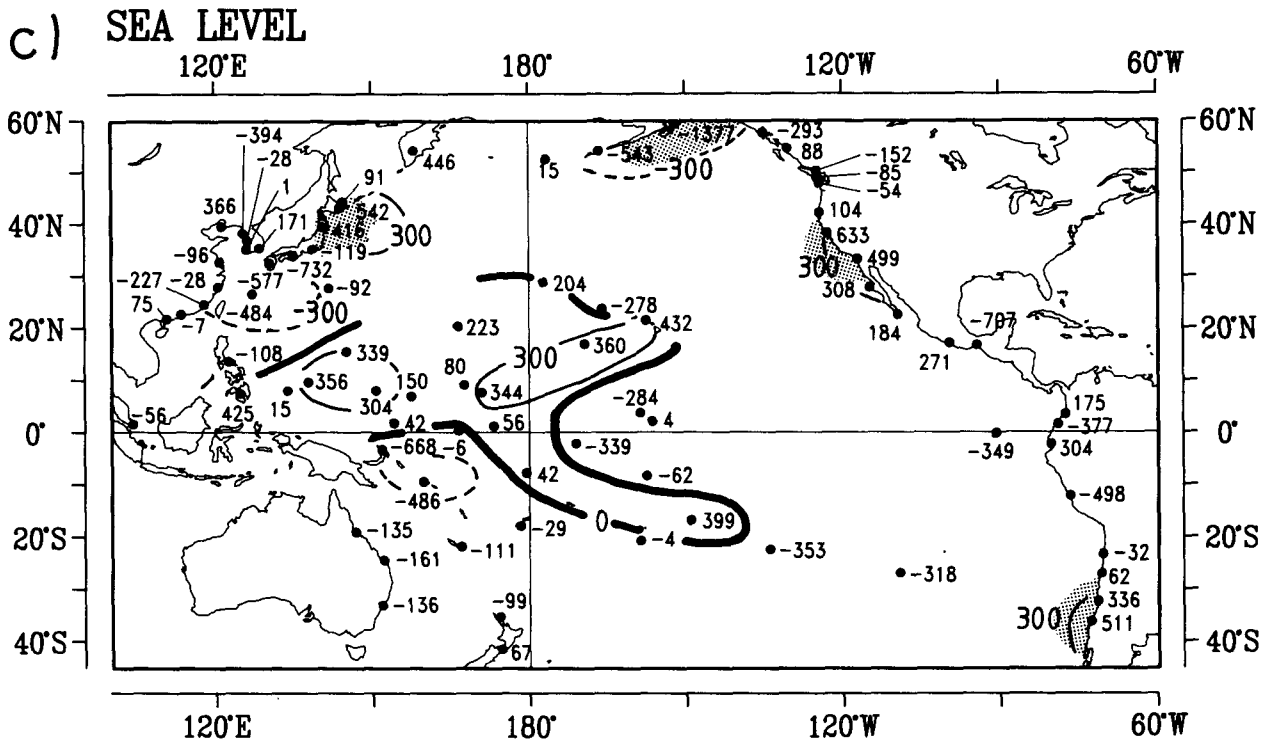

FIG. 10. (*Continued*) (c) Pacific sea level (mm). Shaded areas indicate explained variance larger than 5% for temperature and 10% for sea level.

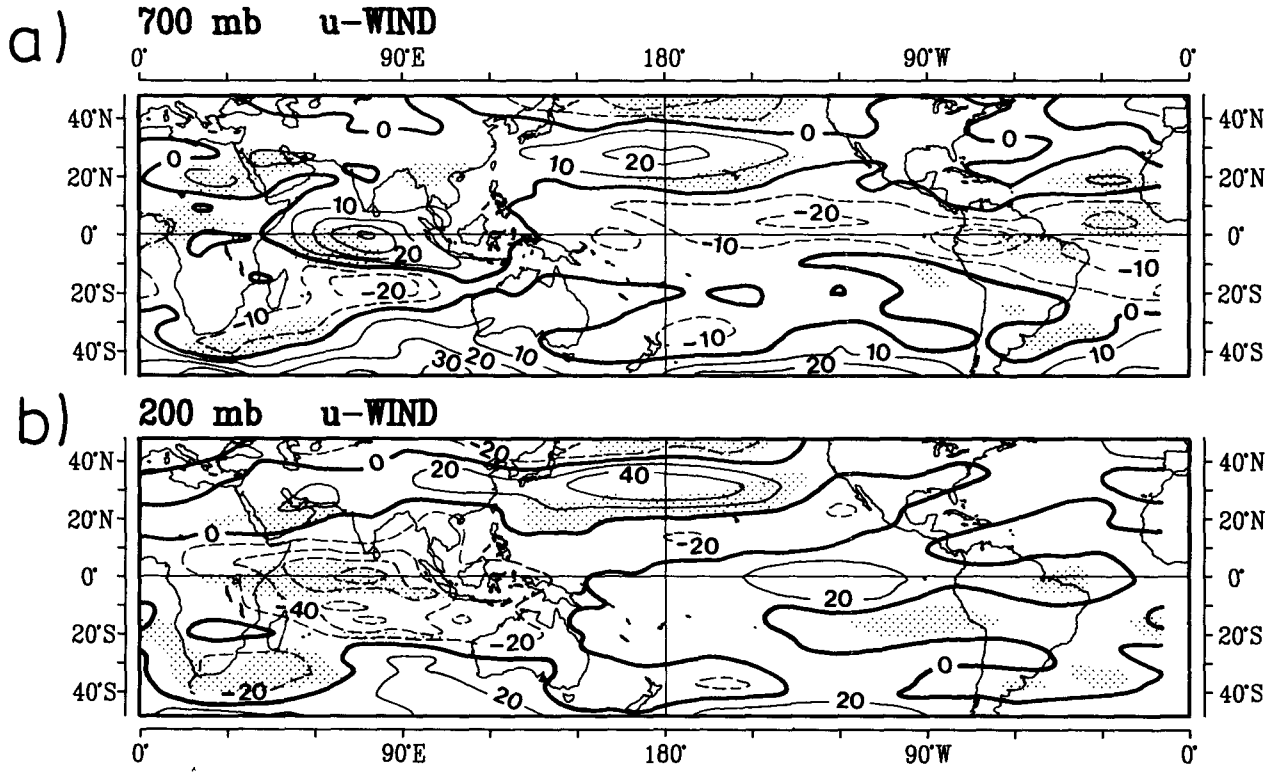

FIG. 11. POP pattern of mode 4 for (a) 700-mb zonal wind (m s^{-1}) and (b) 200-mb zonal wind (m s^{-1}). Shaded areas indicate explained variance larger than 5%.

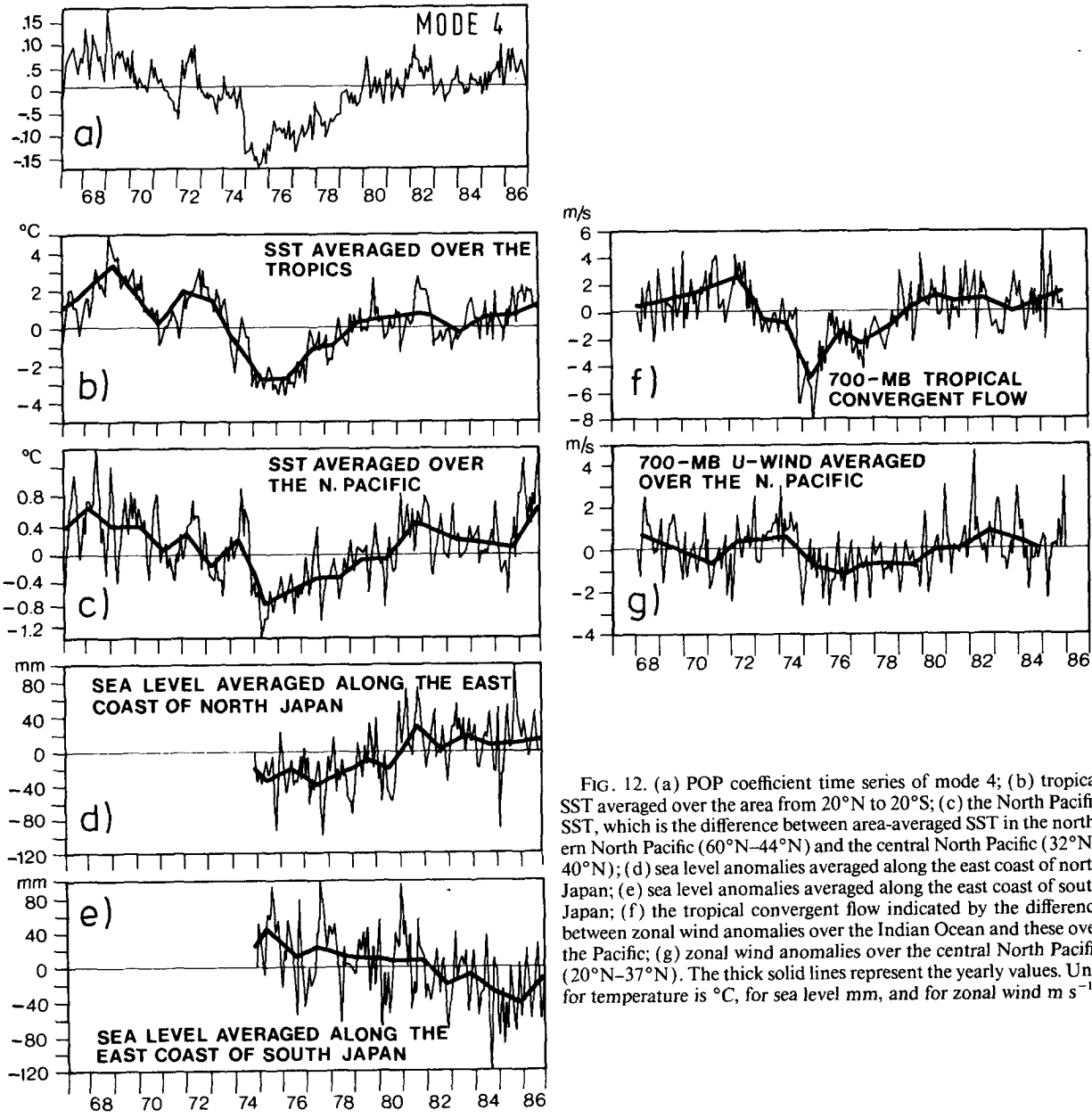

FIG. 12. (a) POP coefficient time series of mode 4; (b) tropical SST averaged over the area from 20°N to 20°S; (c) the North Pacific SST, which is the difference between area-averaged SST in the northern North Pacific (60°N–44°N) and the central North Pacific (32°N–40°N); (d) sea level anomalies averaged along the east coast of north Japan; (e) sea level anomalies averaged along the east coast of south Japan; (f) the tropical convergent flow indicated by the difference between zonal wind anomalies over the Indian Ocean and these over the Pacific; (g) zonal wind anomalies over the central North Pacific (20°N–37°N). The thick solid lines represent the yearly values. Unit for temperature is °C, for sea level mm, and for zonal wind m s^{-1}.

alies in the coastal regions are found (Fig. 10a,c) in the ocean. Certainly the sea level distribution is affected by the scarcity of data in the oceanic interior. Nevertheless, there are interesting patterns along the coast of Japan with negative anomalies in the south and positive anomalies in the north.

Is it possible that these atmospheric and oceanic changes are related to each other? The wind stress (τ) curl forcing ($-\partial\tau^x/\partial y$) calculated from Fig. 11a shows a zero line of $-\partial\tau^x/\partial y$ along 30°N, which is located several degrees south of its climatological position (not shown). According to the Sverdrup relation, anomalous circulation induced by zonal wind patterns such as that shown in Fig. 11a should have anomalous southward (northward) Sverdrup transport south (north) of 30°N, which in turn might generate northward (southward) return flow along the western boundary. The negative (positive) sea level anomalies along the east coast of southern (northern) Japan (Fig. 10c) are consistent with such changes in the Kuroshio and Oyashio currents. Furthermore, the southward displacement of the zero line of curl τ indicates a southward displacement of the water mass associated with this current system. The meridional displacement of the water mass might be related to the zonally oriented SST anomalies along 40°N. The time evolution

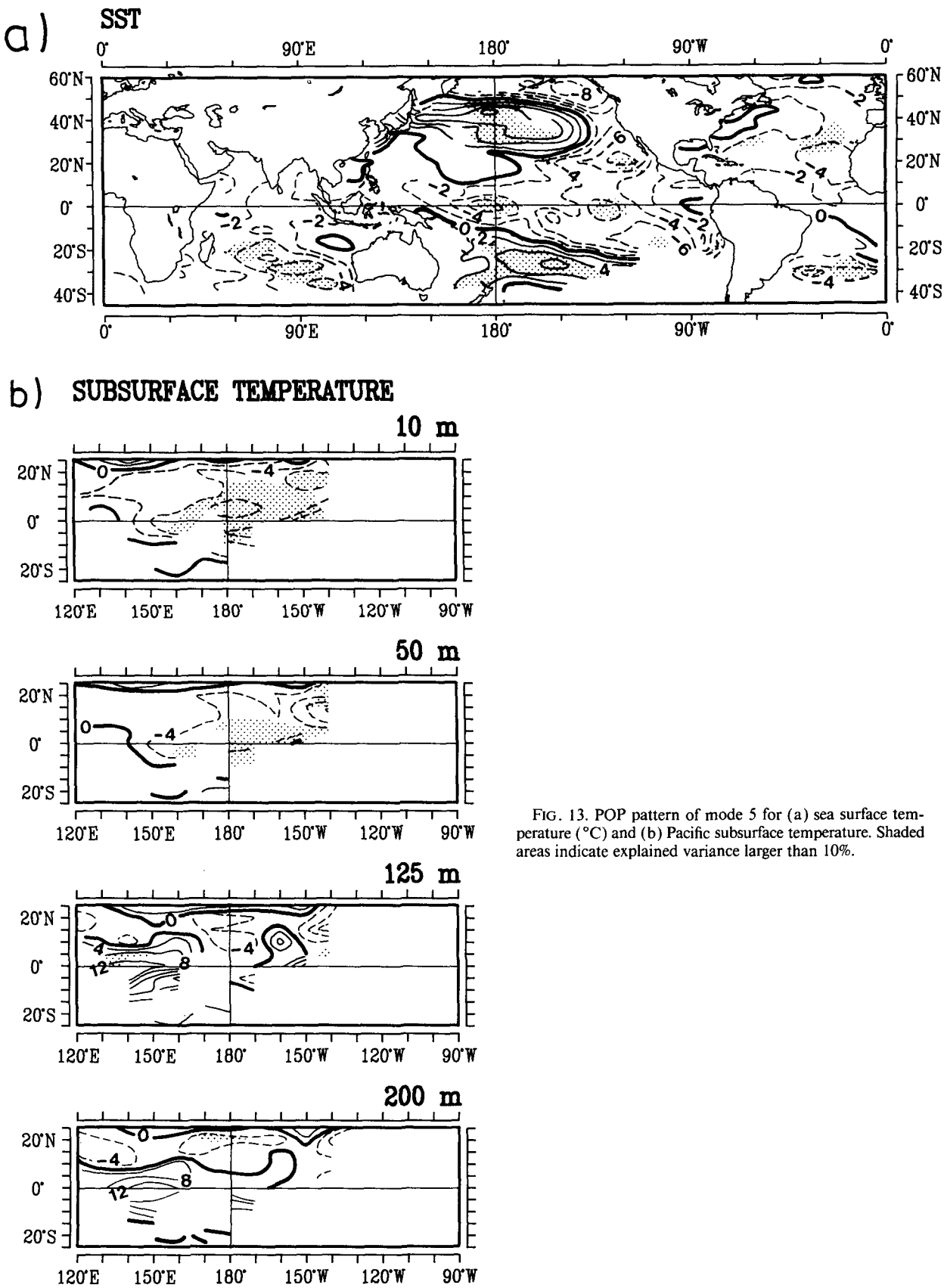

FIG. 13. POP pattern of mode 5 for (a) sea surface temperature (°C) and (b) Pacific subsurface temperature. Shaded areas indicate explained variance larger than 10%.

(Fig. 2d) suggests that the Kuroshio and the Oyashio currents have become stronger since the mid-1970s. This decadal trend in the Kuroshio transport has also been noted by Qiu and Joyce (1992).

The above discussion suggests that the extratropical oceanic anomalies that might be described by changes in the strength and the north- and southward displacement of the subtropical and subpolar gyres in the North Pacific might be induced by wind changes over that area. However, to prove this idea, more data, especially more complete wind and sea level data, are needed.

In order to ensure that mode 4 is not an artifact of the analysis technique, area-averaged time series that characterize the features described above are calculated. Before doing this, other signals in the form of $z_j(t)\mathbf{P}_j$ (j = 1, 2, 3, 5, 6), are subtracted from the raw data $\mathbf{x}(t)$.

Figure 12 shows (a) once again the POP coefficient time series; (b) tropical SST averaged over the area from 20°N to 20°S; (c) the North Pacific SST, which is the difference between area-averaged SST in the northern North Pacific (60°N–44°N) and in the central North Pacific (32°N–40°N); (d) sea level averaged along the east coast of northern Japan; (e) sea level averaged along the east coast of southern Japan; (f) the convective flow indicated by the difference between zonal wind anomalies over the Indian Ocean and those over the Pacific; and (g) zonal wind anomalies over the central North Pacific (20°N–37°N).

It is obvious from Fig. 12 that the tropical and extratropical features described above indeed develop parallel to each other. The strength of the signal is of order of tenths of a degree Celcius for temperature, a few centimeters for sea level, and a few meters per second for zonal winds, as also given by $z_4\mathbf{P}_4$.

The relationship between the convective changes in the tropics and changes in the extratropical tropospheric circulation has been proposed by Flohn et al. (1990). The results shown in this section suggest a more detailed and complex picture of this relationship. However, numerical studies are required for understanding this relationship in the coupled system.

c. *The joint mode on decadal time scales: Mode 5*

The time series of mode 5 shown in Fig. 1e reveals a rather sharp jump during 1975/76. The pattern shown in Fig. 13a indicates that mode 5 is connected with large-scale SST changes, namely, negative anomalies in most parts of the Atlantic and the Indian Ocean, and out-of-phase structure in the Pacific which has negative values in the tropics and positive values in the subtropics. In contrast to mode 4, where large explained variance is confined to the Pacific, mode 5

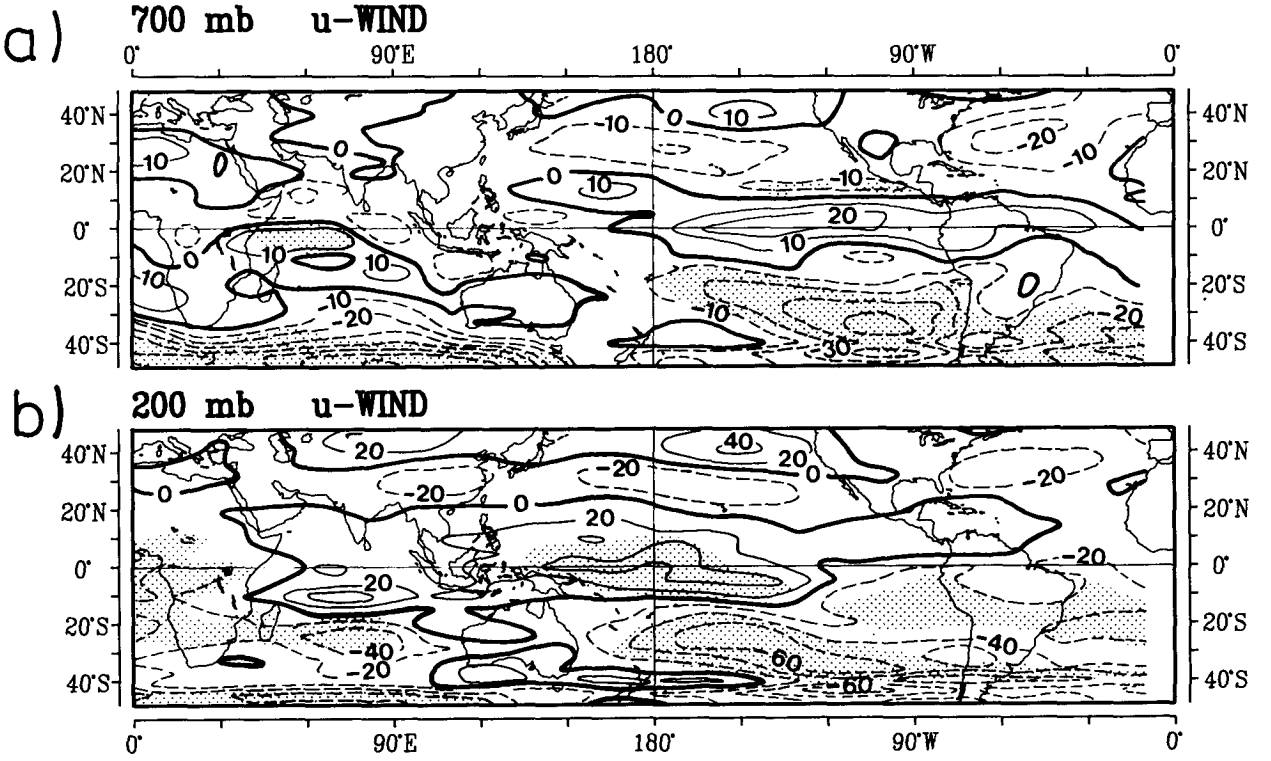

FIG. 14. POP pattern of mode 5 for (a) 700-mb zonal wind (m s^{-1}) and (b) 200-mb zonal wind (m s^{-1}). Shaded areas indicate explained variance larger than 10%.

shows large explained variance in SST in all three oceans (shaded areas in Fig. 13a).

The vertical structure of oceanic anomalies, indicated by the subsurface temperature in Fig. 13b, resembles that of mode 4. No signal (in terms of explained variance) is found in sea level.

For the atmospheric parameter, maxima of anomalies and explained variance are found mostly in the Southern Hemisphere at both 700 and 200 mb (Fig. 14). In the tropics, a large-scale organized convection pattern is not observed. In the Southern Hemisphere, easterly anomalies are found over the southern oceans

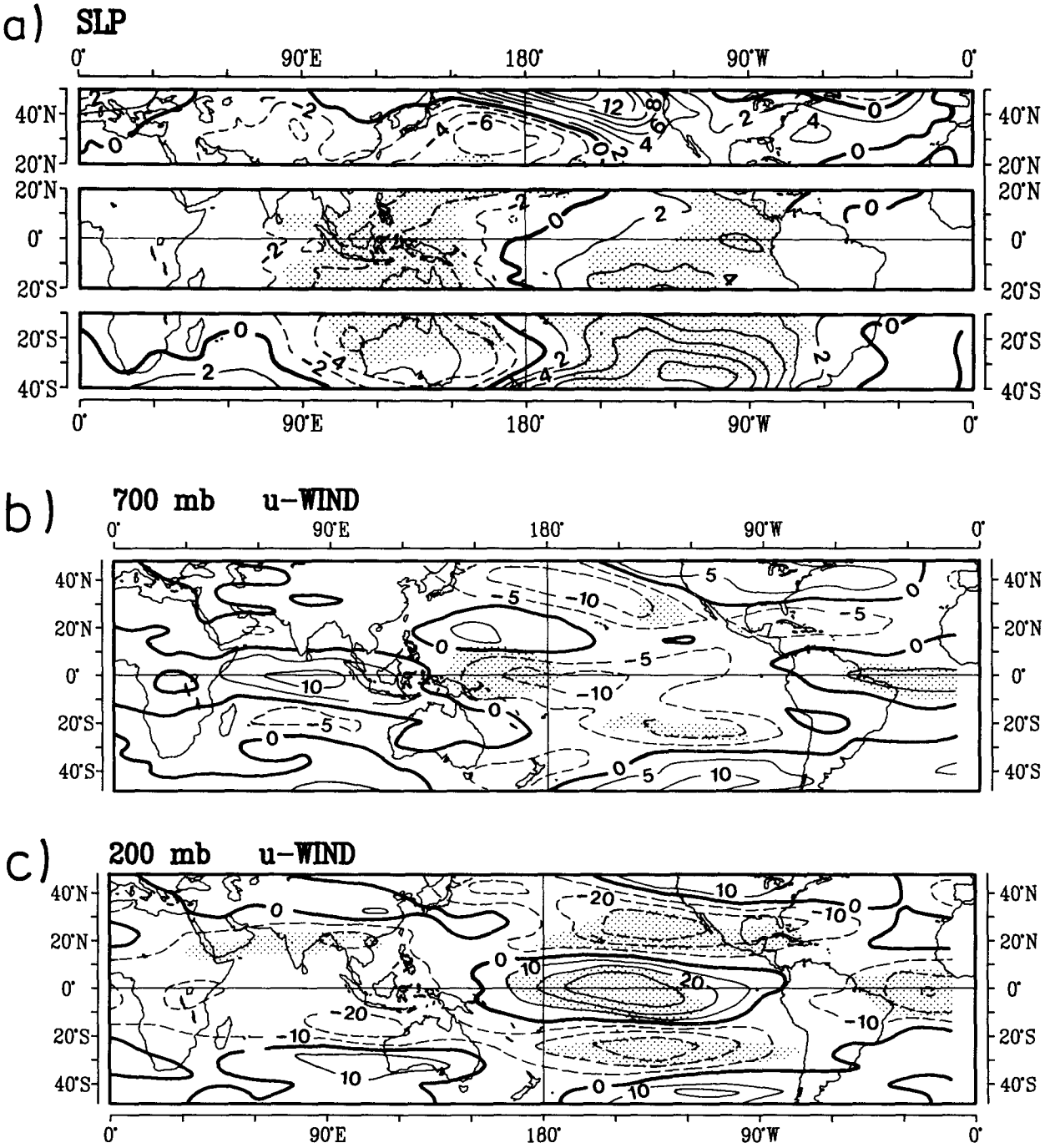

FIG. 15. POP pattern of the imaginary part of mode 6 for (a) sea level pressure (in mb); (b) 700-mb zonal wind (m s^{-1}); and (c) 200-mb zonal wind (in m s^{-1}). Shaded areas indicate explained variance larger than 15%.

except for a small area in the western South Pacific near 40°S. The mean Southern Hemispheric winter circulation as described by van Loon (1972) is characterized by a strong westerly jet along 45°–50°S with maximum values over the south Indian Ocean and South Atlantic, and a double jet structure in the western South Pacific with minimum values along 40°S. Figure 1e indicates that this mean circulation pattern changed very rapidly during 1975/76, with an anomalous weak jet over the southern Indian Ocean and the South Atlantic and an anomalous weak double jet structure over the western part of the South Pacific during the first

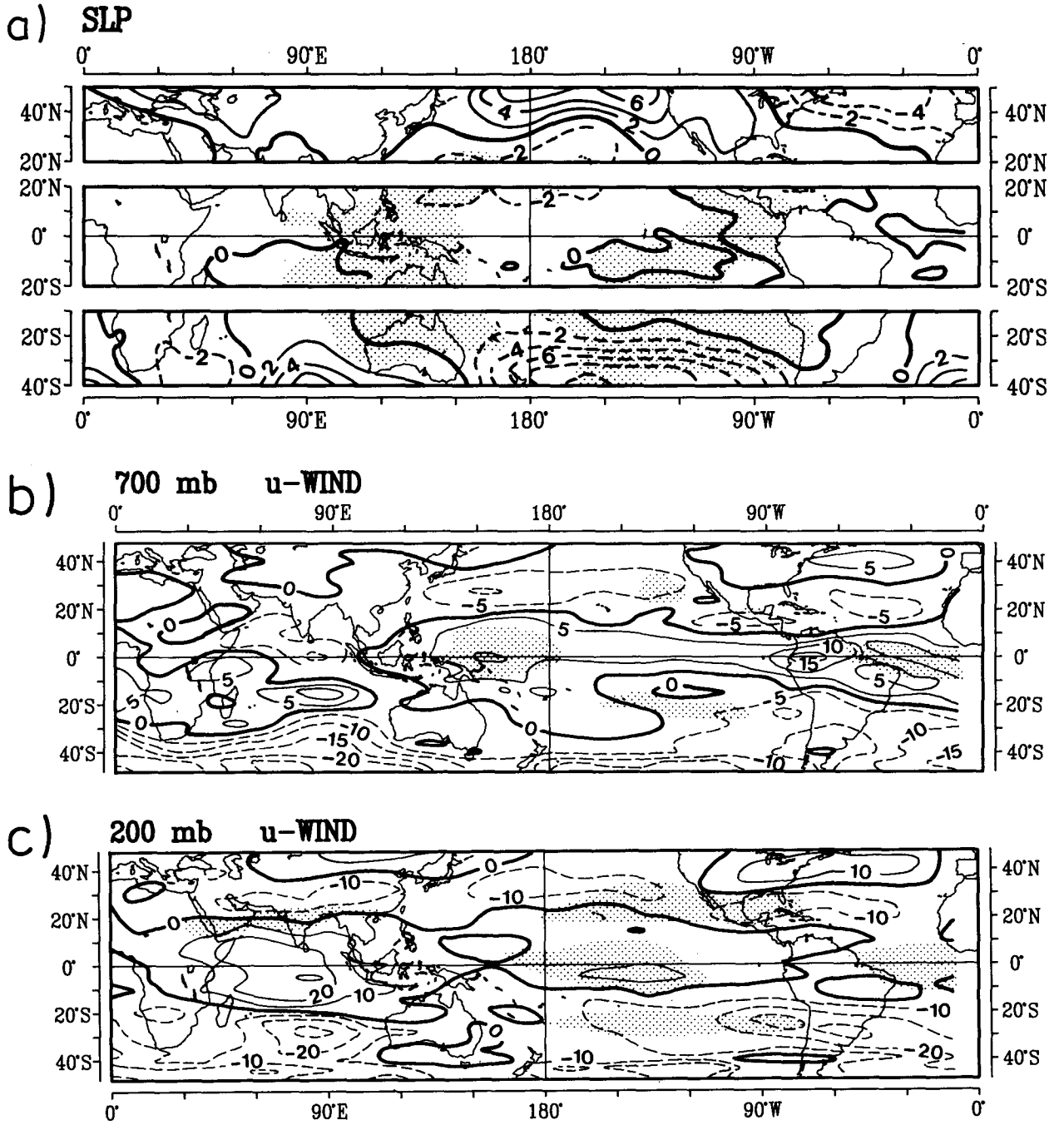

FIG. 16. POP pattern of the real part of mode 6 for (a) sea level pressure (in mb); (b) 700-mb zonal wind (m s^{-1}); and (c) 200-mb zonal wind (m s^{-1}). Shaded areas indicate explained variance larger than 15%.

half of the time period, and an anomalous strong jet and strong double jet structure during the second half of the period.

No air–sea process of the type summarized in section 3 can be identified for mode 5. It is not clear at this stage how and why the global-scale SST anomalies (Fig. 13a) and the changes in the Southern Hemisphere circulation (Fig. 14) are related to each other.

d. The joint oscillatory mode: Mode 6

The complex mode 6 describes the El Niño–Southern Oscillation phenomenon. As mentioned in section 2, a complex POP is defined only to an arbitrary complex factor $e^{i\theta}$. To simplify the interpretation, θ is chosen so that the imaginary part of the POP coefficient time series is maximally correlated (0.72) with the conventional Southern Oscillation index (pressure difference between Tahiti and Darwin). Therefore, the imaginary part of the POP, noted as $\mathbf{P}^{im}$, describes the anomalies associated with the cold extreme of the ENSO phenomenon, and the real part, noted as $\mathbf{P}^{re}$, corresponds to the intervening phase, that is, conditions that appear about one year before a warm extreme.

1) ATMOSPHERIC AND OCEANIC FEATURES OF THE MODE 6

For SLP, the evolution from a cold extreme to a warm extreme is described by an eastward migration of the negative anomalies from the Indian Ocean and the west Pacific during a cold extreme ($\mathbf{P}^{im}$ in Fig. 15a), into the west and central Pacific during the intervening phase ($\mathbf{P}^{re}$ in Fig. 16a), and finally into the central and east Pacific during the warm extreme ($-\mathbf{P}^{im}$). Associated with this evolution an eastward migration of low-level westerly wind anomalies is observed with anomalous westerlies propagating from the Indian Ocean in Fig. 15b into the west Pacific in Fig. 16b and into the central Pacific. At 200 mb the conditions during the extreme phase (Fig. 15c) are well known with strong anomalous westerlies over the central Pacific on the equator and the anomalous easterlies in the subtropical Pacific, whereas during the intervening phase (Fig. 16c) westerlies are found over most of the tropical oceans. It seems that the migration feature is more pronounced at the lower than at the higher level.

The maximum of variance explained by this cyclic evolution is shown by the shaded areas in Figs. 15 and 16. For SLP, the signal in the Southern Hemisphere is stronger than that in the Northern Hemisphere. For the wind, the signal is strong in the west and central Pacific at 700 mb, and over the central Pacific and the subtropical South and North Pacific at 200 mb. The explained variance for both the low- and high-level parameters shows maximal values up to about 35% along the equator and decreases rapidly poleward, especially for SLP and the 700-mb zonal winds.

In the ocean, there is little evidence of migration in the SST (Figs. 17a, 18a). But in terms of the ocean temperature and sea level (Fig. 17b,c and Fig. 18b,c), propagation of anomalies is clearly presented. The sea level anomalies during a cold event ($\mathbf{P}^{im}$ in Fig. 17c) are associated with large positive values over the west Pacific, which has a larger extension north of the equator than south of the equator. On the equator there is a minimum of positive anomalies in the west part of the Pacific and a tongue of negative anomalies in the central and east Pacific. In the intervening stage ($\mathbf{P}^{re}$ in Fig. 18c), the positive sea level anomalies have now moved into the west and central Pacific. The same evolution with even more detailed distribution is shown for the Pacific Ocean temperature in Figs. 17b and 18b. The largest temperature anomalies are reached during a cold extreme in the west Pacific at about 5°S at 200 m deep, and at about 5°N–10°N at 125 m deep. They then migrate equatorward and are located on the equator in the west central Pacific during the intervening stage.

Explained variances larger than 30% for sea level and larger than 30% for temperature are shown by shaded areas in Figs. 17 and 18. As in the case of atmospheric parameters, largest values are located in the equatorial regions.

2) AIR–SEA INTERACTIONS INVOLVED IN MODE 6

The fact that ENSO appears as an oscillatory mode of the atmosphere–ocean system is consistent with previous studies. The well-defined mode in the tropical Pacific, suggested as being a delayed oscillation mode (Suares and Schopf 1988), and also found in an ocean GCM (Latif and Flügel 1991), displays similar sea level evolution to that given by the oscillatory mode 6; the positive sea level anomalies located off the equator in the west Pacific and the tongue of negative sea level anomalies in the equatorial central and eastern Pacific in $\mathbf{P}^{im}$ (Fig. 17c) resemble the sea level anomalies associated with westward-propagating Rossby waves and eastward-propagating Kelvin waves; and the positive anomalies in $\mathbf{P}^{re}$ (Fig. 18c) seem to have been reflected at the western boundary and appear as a Kelvin wave signal centered along the equator. Also, the atmospheric part of the evolution is consistent with that shown first by Barnett (1985, 1988). However, the POP analysis of the combined dataset suggests a new aspect of the atmosphere–ocean behavior in that the oceanic variability is tied to the propagating features of the atmospheric anomalies.

The relation between the atmospheric and the oceanic propagating features appears to be the following. The sea level anomalies in both the extreme phase and the intervening phase might be produced by

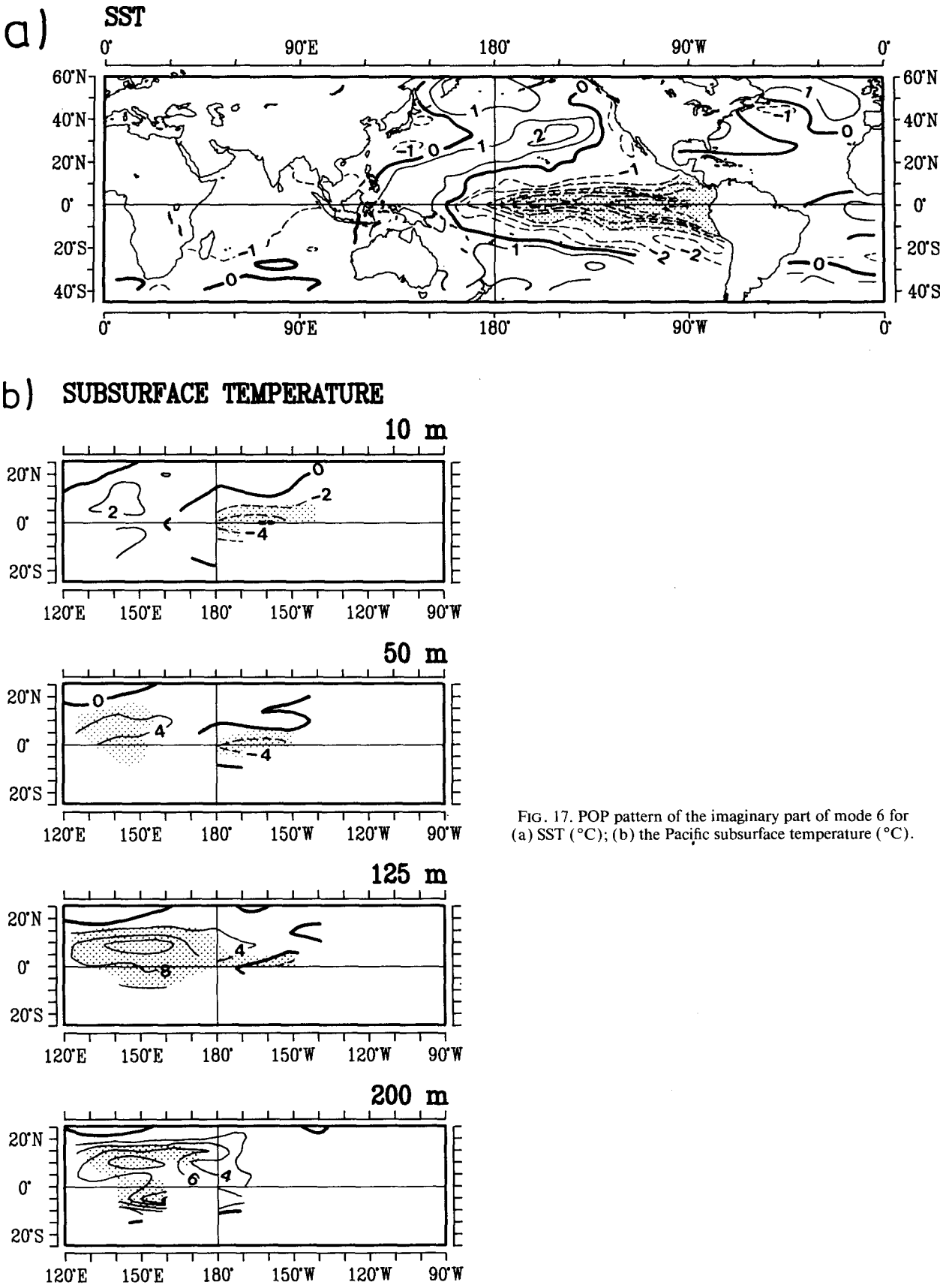

FIG. 17. POP pattern of the imaginary part of mode 6 for (a) SST (°C); (b) the Pacific subsurface temperature (°C).

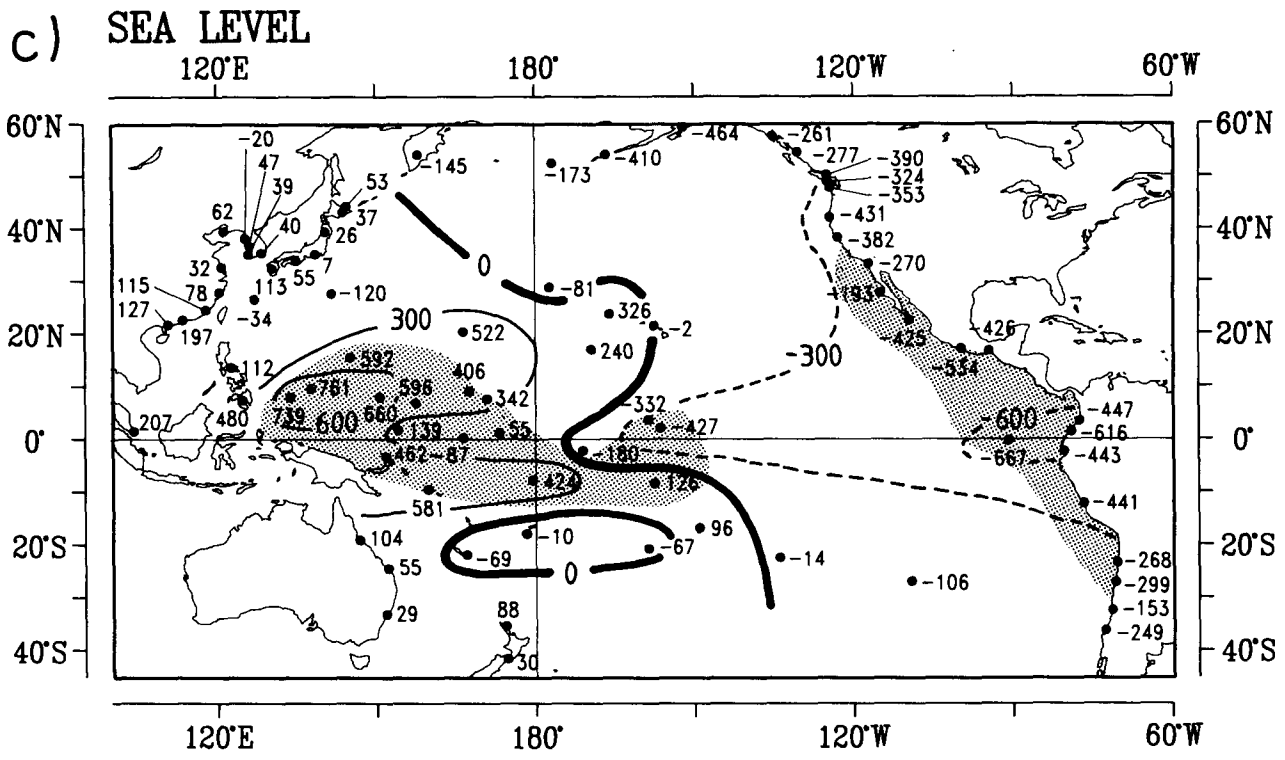

FIG. 17. (*Continued*) (c) Pacific sea level (mm). Shaded areas indicate explained variance larger than 30%.

anomalous atmospheric conditions: the sea level pattern in Fig. 17c by easterly anomalies over the tropical Pacific (Fig. 15b), and the sea level pattern in Fig. 18c by westerly anomalies over the west Pacific (Fig. 16b). It is speculated that the cyclic evolution of oceanic anomalies can be interpreted as the oceanic response to the eastward movement of the low-level zonal wind anomalies.

What is the reason for the cyclic evolution of the wind anomalies? As discussed in section 3, SST is the only forcing for the overlying atmosphere in this context. During the extreme phase, a comparison between SST in Fig. 17a and wind patterns in Fig. 15 indicates that atmospheric anomalies appear in response to the heating anomalies with anomalous convection (an expression of low-level convergence and upper-level divergence) sitting over the warm water in the west during the cold phase and in the east during the warm phase. But during the intervening phase, no notable SST anomalies can be related to the anomalous westerlies over the west Pacific. This indicates that the movement of the wind anomalies is not forced by the SST.

6. Discussion and conclusions

a. Estimated normal modes

As discussed in section 2, POPs are eigenvectors of a system matrix **B**, which is estimated from data. For the example of atmospheric medium-scale traveling waves, Schnur et al. (1993) studied the eigenvectors of a system matrix **B**, which was obtained in two conceptually different ways. In one case **B** was estimated from data (POP analysis), and in the other case it was derived theoretically from the quasigeostrophic equations (normal-mode study by means of a linear stability analysis). Their results show that the POP analysis is able to reveal patterns that are found as normal modes in a theoretical study. Therefore it seems reasonable to interpret the POPs presented in section 5 as "estimated normal modes." There is no proof that these modes are equivalent to normal modes of the coupled atmosphere–ocean system. But the assumption (1) suggests that the POPs are modes that reflect the linear structure of the coupled system. One possibility of deriving the corresponding modes is to estimate them from data.

A disadvantage in estimating normal modes from data is that the physical processes involved cannot be determined by the analysis procedure. For the normal modes found here, associated physical processes are suggested in terms of the information summarized in section 3. More data and other theoretical studies are needed to prove the results.

Besides the brevity and scarcity of data and uncertainties in the question of signal-to-noise ratio, the results suggest that in terms of the amplitude of the POP coefficient time series, the strongest mode in the cou-

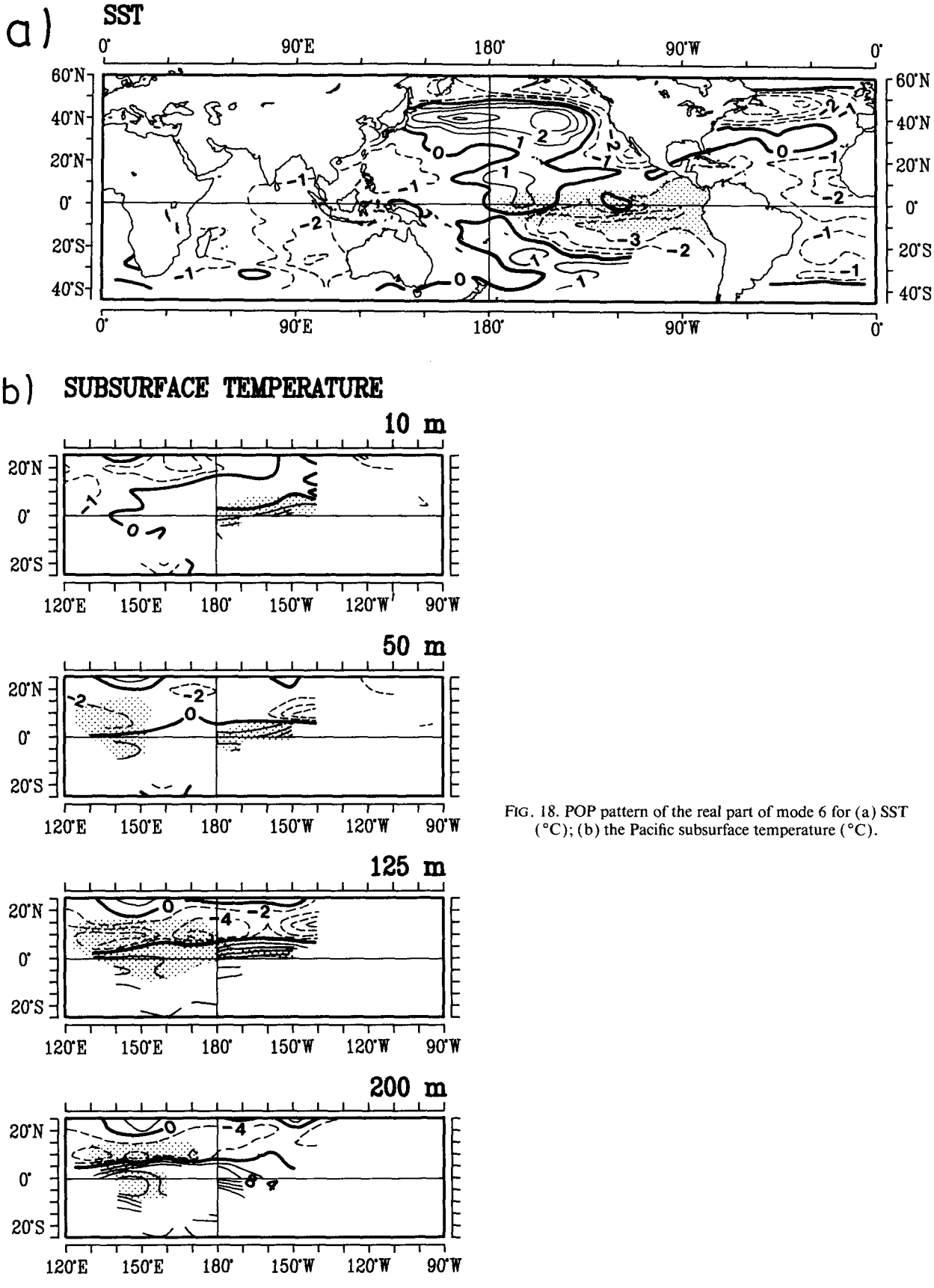

FIG. 18. POP pattern of the real part of mode 6 for (a) SST (°C); (b) the Pacific subsurface temperature (°C).

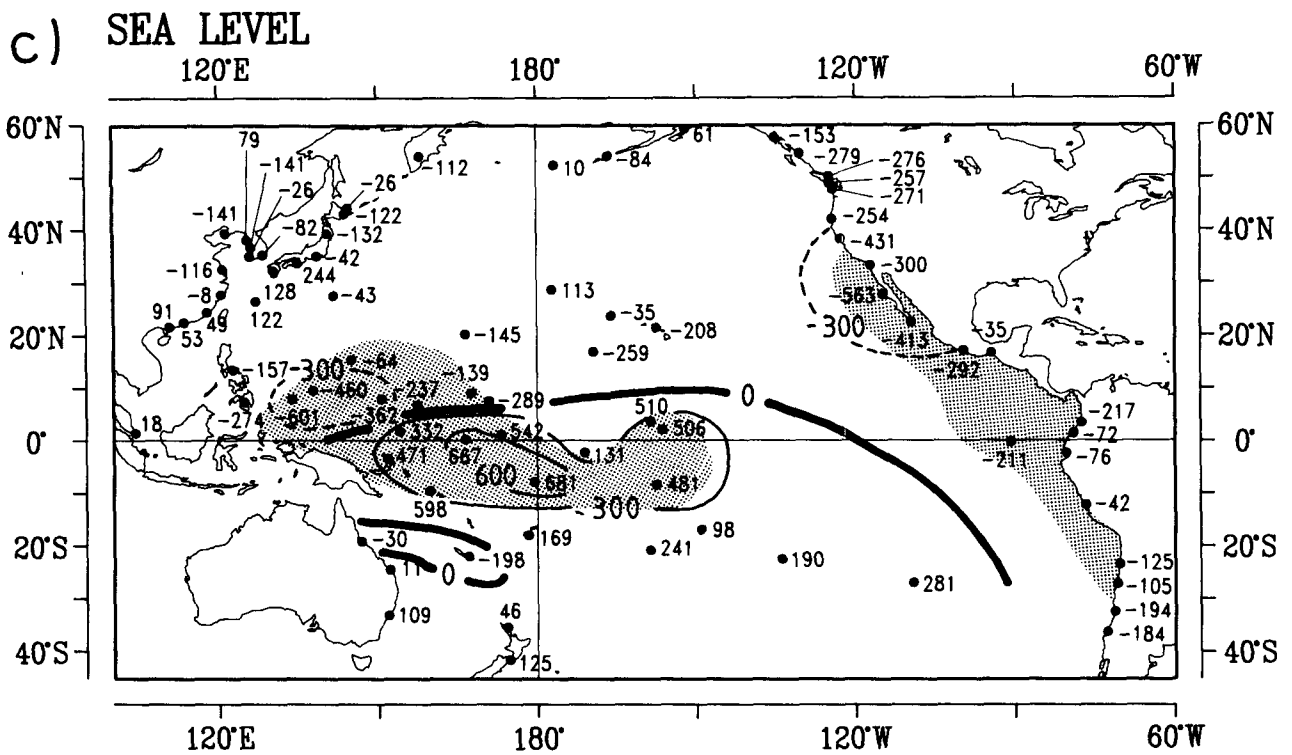

FIG. 18.(*Continued*) (c) Pacific sea level (mm). Shaded areas indicate explained variance larger than 30%.

pled system is the El Niño–Southern Oscillation (mode 6). Among the modes with small eigenvalues (modes 1, 2, and 3), the mode with large anomalies over the Pacific (mode 2) is stronger than the modes with anomaly maxima over the Atlantic. For modes with large eigenvalues (on decadal time scales), the mode associated with changes of tropical SST (mode 4) is stronger than the mode with large wind anomalies over the Southern Hemisphere (mode 5).

b. Multivariate spectral analysis

The agreement between the spectrum given by an eigenvalue or derived from the corresponding POP coefficient time series clearly demonstrates the ability of the POP analysis to pick out the spatially coherent modes together with their spectral features summarized by the eigenvalues.

c. Air–sea processes on different time scales

The results of section 5 indicate that different air–sea processes are involved in different modes. While the atmosphere is responsible for the modes that vary on month-to-month time scales, the role of the ocean becomes more important for the modes that vary on much longer time scales.

On month-to-month time scales, extratropical oceanic anomalies can be understood to be forced by large-scale extratropical atmospheric anomalies. The SST anomalies are mainly caused by anomalous warm and cold air advection and sea level anomalies appear to be produced by the inverse barometric effect.

On decadal time scales, one air–sea process described in section 5 seemed to have its origin in the tropics. This mode shows large-scale SST anomalies in all three tropical oceans and organized convection over the tropical west Pacific. A further investigation of the patterns allows the speculation that this tropical variation could induce changes in the extratropical tropospheric circulation and these might cause changes in the subtropical and subpolar gyres in the North Pacific.

On ENSO time scales, cyclic oceanic anomalies appear to be tied to the eastward propagation of the atmospheric anomalies. However, the results indicate that oceanic forcing in terms of SST is present only during the extreme phase of ENSO, but not during the intervening phase.

Acknowledgments. I would like to express my gratitude to Klaus Hasselmann for his inspiration to explore this topic. I would also like to thank Dennis Moore and Klaus Wyrtki for their suggestions about oceanic anomalies. Many thanks to Grant Branstator, Hans von Storch, Mojib Latif. Ute Luksch, Nanne

Weber, Ernst Maier-Reimer, Jörg-Olaf Wolff, Eduardo Zorita, Gerd Bürger, and George Boer for many fruitful discussions. Thanks also to M. Grunert and D. Lewandowsky for preparing the diagrams, to P. B. Wright for editing the English, and to Jutta Bernlöhr and Heike Schriever for typing the manuscript.

REFERENCES

Barnett, T. P., 1985: Variations in near-global sea level pressure. *J. Atmos. Sci.*, **42,** 478–501.

Barnett, T. P., 1988: Variations in near-global sea level pressure: Another view. *J. Climate,* **1,** 222–230.

Bjerknes, J., 1962: Synoptic survey of the interaction between sea and atmosphere in the North Atlantic. *Geofys. Publ.*, **24,** 116–145.

Egger, J., 1977: On the linear theory of the atmospheric response to sea surface temperature anomalies. *J. Atmos. Sci.*, **34,** 603–614.

Flohn, H., A. Kapala, H.-R. Knoche, and H. Mächel, 1990: Recent changes of tropical water and energy budget and of midlatitude circulations. *Climate Dyn.*, **4,** 237–252.

Hasselmann, K., 1988: PIPs and POPs: The reduction of complex dynamical systems using principal interaction and oscillation patterns. *J. Geophys. Res.*, **93,** 11 015–11 021.

Gill, A. E., 1980: Some simple solutions for heat-induced tropical circulation. *Quart. J. Roy. Meteor. Soc.*, **106,** 447–462.

Gill, A. E., and P. P. Niiler, 1973: The theory of seasonal variability in the ocean. *Deep-Sea Res.*, **20,** 141–177.

Latif, M., and M. Flügel, 1991: An investigation of short-range climate predictability in the tropical Pacific. *J. Geophys. Res.*, **96,** 2661–2673.

Luksch, U., and H. v. Storch, 1992: Modelling the low-frequency sea surface temperature variability in the North Pacific. *J. Climate,* **5,** 893–906.

Qiu, B., and T. M. Joyce, 1992: Interannual variability in the mid- and low-latitude western North Pacific. *J. Phys. Oceanogr.*, **22,** 1062–1079.

Schnur, R., G. Schmitz, N. Grieger, and H. v. Storch, 1993: Normal modes of the atmosphere as estimated by principal oscillation patterns and derived from quasi-geostrophic theory. *J. Atmos. Sci.*, **50,** in press.

Simmons, A. J., J. M. Wallace, and G. W. Branstator, 1983: Barotropic wave propagation and instability and atmospheric teleconnection patterns. *J. Atmos. Sci.*, **40,** 1363–1392.

Storch, H. v., T. Bruns, I. Fischer-Bruns, and K. H. Hasselmann, 1988: Principal oscillation pattern analysis of the 30 to 60 day oscillation in a GCM. *J. Geophys. Res.*, **93,** 11 022–11 036.

Suarez, M., and P. S. Schopf, 1988: A delayed action oscillator for ENSO. *J. Atmos. Sci.*, **45,** 3282–3287.

van Loon, H., 1972: Wind in the Southern Hemisphere. *Meteorology of the Southern Hemisphere,* C. W. Newton, Ed., Meteor. Monogr., No. 35, Amer Meteor. Soc. **35,** 87–100.

Wallace, J. M., and D. S. Gutzler, 1981: Teleconnections in the geopotential height field during the Northern Hemisphere winter. *Mon. Wea. Rev.*, **109,** 784–812.

Webster, P., 1981: Mechanism determining the atmosphere response to sea surface temperature anomalies. *J. Atmos. Sci.*, **38,** 554–571.

Woodruff, S. D., R. J. Sultz, R. L. Jenne, and P. M. Steurer, 1987: A comprehensive ocean–atmosphere data set. *Bull. Amer. Meteor. Soc.*, **68,** 1239–1250.

Wright, P. B., J. M. Wallace, T. P. Mitchell, and C. Deser., 1988: Correlation structure of the El Niño/Southern Oscillation Phenomenon. *J. Climate,* **1,** 609–625.

Wyrti, K., K. Constantine, B. J. Kilonsky, G. Mitchum, B. Miyamoto, T. Murphy, S. Nakahara, and P. Caldwell, 1988: The Pacific Island sea level network. JIMAR Contrib. 88-0137, Data Rep. 002, Univ. of Hawaii, Honolulu, 71 pp. [Available from University of Hawaii, JIMAR, 1000 Pope Rd., MSB 312, Honolulu, HI 96822.]

Xu, J., 1992: On the relationship between the stratospheric quasi-bienniel oscillation and the tropospheric Southern Oscillation. *J. Atmos. Sci.*, **49,** 725–734.

——, and H. v. Storch, 1990: Predicting the state of the Southern Oscillation Using Principal Oscillation Pattern Analysis. *J. Climate,* **3,** 1316–1329.

Zorita, E., V. Kharin, and H. v. Storch, 1992: The atmospheric circulation and sea surface temperature in the North Atlantic area in winter: Their interaction and relevance for Iberian precipitation. *J. Climate,* **5,** 1097–1108.